On the Controllability and Observability of Flexible Beams Under Rigid-Body Motion

by

Kyung Sang Cho

B. Eng. (Sung Kyun Kwan Univerisity, Seoul), 1988

Department of Mechanical Engineering

McGill University, Montreal

Canada

A thesis submitted to the Faculty of Graduate Studies and Research

in partial fulfillment of the requirements for the degree of

Master of Engineering

August 5, 1991

Abstract

This thesis considers the transverse vibrational control of a single flexible beam undergoing large planar rotational motion. The beam is modelled using a cubic spline technique, which approximates the linearly elastic, continuous beam with a finite number of nodal points. It is shown that kinetic boundary conditions such as those associated with tip loads can be included in the cubic spline model. This spatial discretization method provides a useful linear relationship between displacement and curvature, which allows the use of strain gages to measure curvature along the beam. An optimal control strategy is used to suppress the transverse vibrations while forcing the end tip to follow a prescribed trajectory. A Kalman filter is employed to optimally estimate state variables which are not obtained through direct measurement. These state variables can be classified into two groups: 1) state variables corresponding to the time rate of change of curvature, which cannot be measured using any existing sensor and 2) state variables associated with curvature at certain nodal points which, by having their values estimated rather than directly measured, results in a smaller number of sensors needed to control the entire beam, thereby reducing the required data throughput capability and cost of the control hardware. Although, in principle, the entire system has been proven to be state controllable and observable using as little as one sensor, numerical ill conditioning of the controllability and observability matrices can prevent the Kalman filter from reconstructing the state estimates to a required accuracy. Thus, numerical viability of this control scheme is demonstrated through extensive simulation studies and guidelines for the number and location of sensors to achieve good numerical conditioning are given. These results show that the proposed approach is very suitable for real time control of transverse vibrations of the flexible beam undergoing large rotational motion at high speed.

Résumé

Dans ce mémoire l'auteur, étudie le commande de la vibration transversale d'une poutre flexible, en présence de grands mouvements de rotation dans un plan. La poutre est construite selon une technique de splines cubiques, laquelle sert à obtenir une approximation d'une poutre continue, linéairement élastique, ayant un nombre fini de points nodaux. On démontre que les conditions cinétiques de frontière, telles que celles reliées au fait d'avoir une masse à une extrêmité, peuvent se trouver dans le modèle de spline cubique. Cette méthode de discrétisation spatiale procure une relation linéaire utile entre le déplacement et la courbure, permettant ainsi l'utilisation de jauges extensométriques pour mesurer la courbure le long de la poutre. On utilise une stratégie de commande optimale pour réprimer les vibrations transversales, pendant que l'on force l'extrêmité à suivre une trajectoire imposée. On emploie un filtre de Kalman pour une estimation optimale des variables d'état, laquelle n'est pas obtenue par mesurage direct. Ces variables peuvent être classées en deux groupes: 1) variables correspondant à la vitesse de changement de la courbure, laquelle ne peut être mesurée actuellement par aucun capteur 2) variables associées à la courbure à certains points nodaux, dont la valeur étant estimée au lieu d'être mesurée directement, fait qu'un très petit nombre de capteurs est nécessaire pour commander totalement la poutre. Ce fait a pour conséquence de réduire la quantité d'information requise et le coût du matériel de commande. Quoique, en principe, tout le système a démontré qu'il peut être contrôlable et observable en n'utilisant qu'un seul capteur, la mauvaise condition numérique des matrices de contrôlabilité et d'observabilité peuvent empêcher le filtre de Kalman de rétablir les estimations d'état au degré de précision requise. Ainsi, la viabilité numérique de ce plan de commande est démontrée par des nombreuses études de simulation, et des indications sont données concernant le nombre et l'emplacement des capteurs pour atteindre de bonnes conditions numériques. Ces résultats démontrent que l'approche proposée convient très bien pour la commande en temps réel des vibrations transversales d'une poutre flexible soumise à de grands mouvements de rotation à vitesse élevée.

Acknowledgements

I would like to express my gratitude to my research supervisors, Professors J. Angeles and N. Hori, for their support and guidance. I would also like to express my appreciation to all my colleagues and friends in the Department of Mechanical Engineering and in the McGill Research Centre for Intelligent Machines, especially John Darcovich and Robert Lucyshyn, for sharing with me their valuable time. In addition, thanks are due to Irene Cartier for translating the abstract into French. Finally, I am most grateful to my wife for all her precious support and encouragement.

This research work reported here was made possible under NSERC (Natural Sciences and Engineering Research Council) of Canada Grants #A4532 and #A11750, as well as IRIS (Institute for Robotics and Intelligent Systems, a network of Canadian centers of excellence) Project # C-2.

Contents

List of Tables

List of Figures

Chapter 1

Introduction

1.1 Motivation

During the past decade, there have been extensive studies on the modelling and control of light-weight robotic manipulators, to which conventional rigid-body models are no longer applicable. Light-weight manipulators offer advantages such as higher-speed performance, higher payload-to-weight ratio capacity, and lower energy consumption (Book and Majette 1983). Light-weight robotic manipulators may be required to perform such specialized tasks as space-structure construction and satellite maneuvering. However, such light-weight robots have very light natural damping and non-negligible link flexibility, resulting in vibration and bending effects that must be controlled to ensure adequate performance. The development of a proper control strategy requires a suitable finite-dimensional model which takes into account the dynamics of link flexibility and, at the same time, makes on-line control practical. Although a number of approaches exist to control lightweight robotic manipulators, they employ complex dynamic modelling procedures which may not be economical to implement to suppress vibration and bending effects in real-time.

The research reported in this study is motivated by the need to develop a suitable finite-dimensional dynamic model, which can be used to control a flexible beam in real-time, under large rigid-body motions. Using the optimal control scheme, the Kalman filter is employed

to reconstruct state variables with the smallest possible number of measurements

1.2 Previous Work

In theory, the structural members of light-weight robotic manipulators are distributed parameter or continuous systems which require an infinite number of generalized coordinates to completely describe their vibrational behavior. It is therefore difficult to design a controller for this infinite-dimensional system. Various approaches have been proposed to mathematically model and approximate this distributed-parameter system with a finite dimensional model. These approaches can be classified into two types: the first is the normal mode analysis, which neglects higher vibration modes and uses only the first few dominant modes, the second is the finite-element method, which discretizes the continuous system into a finite set of elements on which the displacement field is assumed to take on a simple form, usually as a multivariate polynomial of a low degree (up to three). In addition, recent studies (Dancose Angeles and Hori 1989) employed the cubic-spline spatial discretization method. Each of them are described below in some detail.

1.2.1 The Normal-Mode Analysis

Modelling of the beam is often achieved by the normal-mode analysis whereby the vibration of the beam is expressed as a finite sum of the principal modes obtained by solving eigenfunctions of the system, while taking into consideration the boundary conditions. Control is then accomplished using state-space approaches including the first few dominant vibration modes (Cannon and Schmitz 1984; Sakawa, Matsuno and Fukushima 1987, Book and Majette 1983, Gordon; Benati and Morro 1988). This method is computationally efficient but has a few limitations for modelling and control. First, the normal-mode analysis requires an accurate mathematical model to ensure successful non-collocated control, where the position of one end is to be sensed and precisely positioned by the application of the torque at the hub of the beam. However, the exact mode shape of any physical system is difficult to determine

in practice. Secondly, the normal-mode analysis determines the natural modes of a uniform beam by finding the eigenfunctions of the governing partial differential equation. While this technique is applicable to uniform beams, it is not suitable for nonuniform beams such as those present in robotic manipulator links. Moreover, the measurement of certain state variables often requires the use of a vision system which, although suitable for end point-tracking control, is too slow at present for transverse vibration control of the entire beam. Finally, this end-point sensing gives non-minimum phase problems, resulting in unstable zeros, due to the non-collocated sensors and actuators, making it unsuitable for systems undergoing large rigid body motions (Shchuka and Goldenberg 1989; Totfs, Swevers and De Schutter 1991). In fact, in the work reported by Cannon and Schmitz (1984), the flexible beam is limited to rotate horizontally from 0° to only 6° about its fixed end.

1.2.2 The Finite-Element Method

The other commonly used approach is the finite-element method, which discretizes the continuous beam by dividing the length of the beam into a finite set of smaller beams. Using this method, governing equations of the flexible beam are derived as a set of second-order ordinary differential equations, rather than as a set of partial differential equations. This method allows the modelling of beams which have non-homogeneous material properties, non-uniform cross sections, and a variety of boundary conditions such as hub and tip loads (Bayo 1988; Menq and Chen 1988; Giovagnoni and Rossi 1989). However, the use of finite element methods generally produces a large system of ordinary differential equations to model the system with sufficient fidelity, thereby requiring more expensive computational and control hardware. Moreover, the use of a large number of equations in the associated state-space modelling inevitably introduces non-negligible numerical errors and prevents one from using a high sampling rate for digital control. A high sampling rate is required to ensure that the sampling frequency is larger than at least twice the highest resonant frequency of the system, in order to avoid unacceptable sensitivity to plant disturbances. This technique is suitable, therefore, only for open-loop simulation and may not be adequate for closed loop control design. This method also often uses end-point sensing, which is unsuitable for

control of flexible beams undergoing large rigid-body motions due to their non minimum phase characteristics. It is, therefore, worthwhile examining an alternative approximation techniques, like the one based on cubic splines, which makes on-line control feasible

1.2.3 The Cubic-Spline Technique

A new approach to the modelling of a flexible beam has been introduced by Dancose and et al. (1989). This method employs a cubic-spline technique that approximates the elastica of the continuous beam with a cubic spline passing through various nodal points along the beam. It has been shown that this spatial discretization procedure allows one to model nonuniform and nonsymmetric beams with high accuracy. Also, this method provides a very useful linear relationship between displacement and curvature, thereby allowing the use of accurate and fast strain gages to infer transverse displacement measurements. This is in contrast to other techniques using a computationally expensive vision system to measure end-tip displacement in three-dimensional space.

However, this method does not consider a variety of boundary conditions which are commonly present in robots, such as with tip loads. Moreover, the control of the flexible beam is obtained using an optimal regulator, where a control law is used to drive the state to zero for the given non-zero initial condition. Very rapid decay can be obtained at the expense of large control energy, increasing closed-loop bandwidth and, hence, increasing sensitivity to noise (Kailath 1980). Thus, it may not be applicable to the real-time control of the flexible beam, which requires good transient response to the reference input. Furthermore, the Kalman filter is designed to reconstruct the entire state using all possible measurements, i.e., curvatures at each of the nodal points along the beam and hub rotational angle. However, it is not economical to use all accessible measurements for suppressing vibration of the flexible beam, since this requires a high data throughput capability.

1.3 Objectives

In this thesis, the cubic-spline technique is extended to include the case with a tip mass, while incorporating the associated boundary conditions. An optimal controller, rather than a regulator, is used to suppress the transverse vibration of the entire beam while forcing the end tip to follow a prescribed trajectory. Furthermore, this scheme allows the reference hub angle as well as its velocity profile to be specified for a smooth transient response. Using the Kalman filter, an investigation is also conducted to assess the feasibility of a reduced number of measurements at a selected number of nodal points. Moreover, the problem of sensing, which includes the number and location of the sensors and the selection of the sampling rate, are considered. Finally, the flexible beam, carrying a tip mass and rotating horizontally from 0° to 180° about its fixed end, is simulated to illustrate the effectiveness of the proposed control scheme. This is compared with a simulation of an uncontrolled beam to demonstrate the capability of the control system in suppressing transverse vibrations.

1.3.1 Extended Cubic-Spline Technique

In order to obtain the proper dynamic model of a single link flexible beam performing realistic tasks, the careful consideration of associated boundary conditions must be carried out. One very important example is that of a mass located at the end of the beam, which is considered in detail in this thesis. Typical occurrences of end masses are manipulator payloads and actuators located at the end of each link. Using Hamilton's principle, the governing partial differential equation of the clamped-free beam, along with two geometric boundary conditions and two kinetic boundary conditions, are obtained. The kinetic boundary conditions correspond to the shear force and bending moment caused by the tip mass. The bending moment can usually be neglected due to the low moment of inertia of the tip mass. The shear force can be computed using the tip acceleration, obtained by substituting the cubic spline approximation into the governing partial differential equation. Therefore, the shear force boundary condition and the two geometric boundary conditions can then be included in the formulation of the linear relationship between displacement and curvature.

so that the energy equations of the beam can be determined from the cubic spline equations.

1.3.2 Control Capability

The dynamic model obtained by applying the Euler-Lagrange method is cast into a continuous time, constant-coefficient, state-space description to design an optimal control system. The corresponding step-invariant, discrete-time model is then obtained under the assumption that the control signal is applied to the plant through a zero-order hold. The Kalman filter, which is optimal in the sense that the variance of the estimation error is minimized (Franklin, Powell and Workman 1990; Åström and Wittenmark 1981), is designed to obtain the estimate of the state variables that cannot be directly obtained through measurements. In addition to estimating the time rate of change of curvature, it may be beneficial to estimate the curvature also at certain nodal points, rather than measuring it directly, thereby eliminating the need to use control hardware with very high data throughput capability. Thus, it is of practical importance to find the smallest possible number of measurements which allows the state to be estimated in real-time with a desired accuracy. This reconstruction procedure requires that the system be completely state-observable and controllable to ensure the uniqueness of a feedback gain vector. Although state-observability and controllability have already been theoretically proven in this situation (Balas 1978; Hughes and Skelton 1980), the Kalman filter can fail to allocate the steady-state observer gain matrix due to the numerical ill-conditioning of the controllability and observability matrices. Therefore, to assess the numerical viability of the state estimates obtained by the Kalman filter, extensive simulation studies are performed.

1.3.3 Sensing Considerations

The number of sensors and their positions can significantly affect the dynamic performance of the system and must be taken into consideration in both plant modelling and design and implementation of the control system. The number of sensors, which corresponds to the number of nodal points, is chosen as a compromise between the accuracy of the approximation

and the dimension of the equations of motion which permits real-time implementation of control scheme.

When nearly collocated sensors and actuators are used, that is, when the actuators and sensors are located close to each other, the controller will introduce additional damping to the system, thereby increasing sensitivity to the higher resonant frequency greater than the closed-loop system bandwidth. Therefore, the highest open loop system resonant frequency to be controlled is used as the primary criterion for selecting the best sampling rate as suggested by Franklin et al. (1990).

1.4 Outline of the Remaining Chapters

In Chapter 2, the problem formulation and the spatial discretization of the continuous beam using the cubic-spline method are described, including the application of a variety of boundary conditions. The finite-dimensional equations of motion of the rotating flexible beam are formulated using the Euler-Lagrange equations. In Chapter 3, the step-invariant discrete-time model of the continuous-time, linear, constant-coefficient model of the system in state-variable space is derived. The design of an optimal control system using the Kalman filter is then discussed. In Chapter 4, the determination of the number and location of sensors is discussed based on the state-observability of the system, and the selection of the sampling rate is described. Simulation results are presented and discussed. Finally, in Chapter 5, the results are summarized and suggestions for further work are presented.

Chapter 2

Problem Formulation

The energy-based dynamics modeling of a single flexible beam with a tip mass is achieved by discretizing the linearly elastic, continuous beam using a cubic spline, which approximates the elastica of the continuous beam with a finite number of nodal points. This spatial discretization method is applicable for the determination of the possible boundary conditions and provides a very useful linear relationship between displacement and curvature. This relationship enables the use of fast and accurate strain gages for measuring the curvature along the beam, thereby avoiding the use of complex and computationally expensive vision systems for measuring the tip displacement in the three-dimensional space. The detailed energy equations of the flexible beam, which are obtained by employing the time-varying curvature vector and the cubic-spline approximation, are used to derive the equations of motion using the Euler-Lagrange formulations.

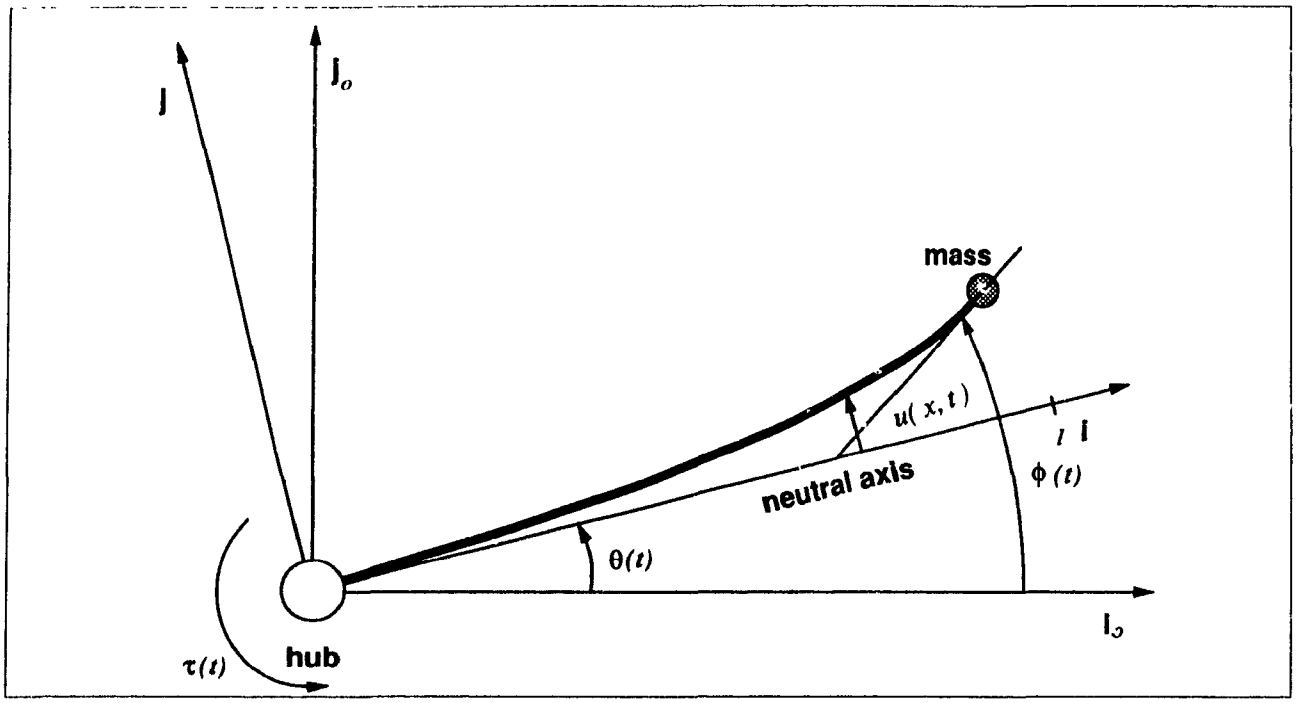

Figure 2.1: Schematic of rotating flexible beam

2.1 Derivation of the Kinetic and Potential Energies

The beam, rotating horizontally about its fixed end with a concentrated tip mass, is modeled as a continuous and clamped-free beam of length l, as shown in Fig. 2.1. The kinetic and potential energies of the beam, denoted by T and V, respectively, are given below:

$$T = \frac{1}{2}\int_0^l \rho(x)s(x) \parallel \dot{\mathbf{r}} \parallel^2 dx + \frac{1}{2}I_h\dot{\theta}^2 + \frac{1}{2}M \parallel \dot{\mathbf{r}} \parallel^2_{x=l} + \frac{1}{2}I_m\dot{\phi}^2 \tag{2.1}$$

$$V = \frac{1}{2}\int_0^l EI(x,t)[u''(x,t)]^2 dx \tag{2.2}$$

where

l : length of the beam [m]

$\rho(x)$: mass density [kg/m^3]

$s(x)$: cross-sectional area [m^2]

$EI(x)$: flexural rigidity [kg m^3/s^2]

$u(x,t)$: deflection of the beam from its neutral axis [m]

$u''(x,t)$: curvature of the beam [m^{-1}]

I_h : moment of inertia of the hub [kg m^2]

I_m : moment of inertia of the tip mass [kg m^2]

M : tip mass [kg]

θ : rotation angle of the hub [radian]

ϕ : rotation angle of the tip mass [radian]

Now we introduce the assumptions below:

- The deflection $u(x,t)$ is small compared with the length of the beam ($\leq 0.1l$) and any longitudinal extension of the beam is negligible.
- The cross-sectional dimensions are small compared with the length of the beam ($< 0.1l$) and, thus, the rotary inertia effects and shear deformation can be neglected (Timoshenko 1955).
- The centrifugal force of the beam and tip mass can be neglected for the linearized formulation of equations of motion.
- The hub is rigid.

From these assumptions, expressions for the position vector r of an arbitrary point on the

beam along with its velocity $\mathbf{r}$ and its velocity magnitude $\| \dot{\mathbf{r}} \|$ are derived from

$$\mathbf{r} = x\mathbf{i} + u\mathbf{j} \tag{2.3}$$

where the unit vectors $\mathbf{i}$ and $\mathbf{j}$, fixed to the hub, are time-varying, whereas $\mathbf{i}_0$ and $\mathbf{j}_0$, shown in Fig. 2.1, are fixed to the inertial frame. Therefore, the position vector $\mathbf{r}$ can be derived with respect to the fixed-frame vectors $\mathbf{i}_0$ and $\mathbf{j}_0$ as shown below:

$$\mathbf{r} = (x\cos\theta - u\sin\theta)\mathbf{i}_0 + (x\sin\theta + u\cos\theta)\mathbf{j}_0 \tag{2.1}$$

$$\dot{\mathbf{r}} = [(\dot{x} - u\dot{\theta})\cos\theta - (x\dot{\theta} + \dot{u})\sin\theta]\mathbf{i}_0 + [(x\dot{\theta} + \dot{u})\cos\theta + (\dot{x} - u\dot{\theta})\sin\theta]\mathbf{j}_0 \tag{2.5}$$

$$\| \dot{\mathbf{r}} \|^2 \equiv \mathbf{r}\cdot\dot{\mathbf{r}} = u^2\dot{\theta}^2 + x^2\dot{\theta}^2 + \dot{u}^2 + 2x\dot{\theta}u. \tag{2.6}$$

The time rate of change $\dot{\phi}$ of the neutral axis of the beam at the end carrying the mass is also obtained from the partial derivative of the position vector $\mathbf{r}$, i.e.,

$$\left.\frac{\partial \mathbf{r}}{\partial x}\right|_{x=l} = (\cos\theta - u'(l,t)\sin\theta)\mathbf{i}_0 + (\sin\theta + u'(l,t)\cos\theta)\mathbf{j}_0 \tag{2.7}$$

$$\begin{aligned}\left.\frac{\partial}{\partial t}\left(\frac{\partial \mathbf{r}}{\partial x}\right)\right|_{x=l} &= (-\dot{\theta}\sin\theta - \dot{u}'(l,t)\sin\theta - u'(l,t)\cos\theta)\mathbf{i}_0 \\ &\quad + (\dot{\theta}\cos\theta + \dot{u}'(l,t)\cos\theta - u'(l,t)\dot{\theta}\sin\theta)\mathbf{j}_0\end{aligned} \tag{2.8}$$

$$\dot{\phi}^2 \equiv \left\| \frac{\partial}{\partial t}\left(\frac{\partial \mathbf{r}}{\partial x}\right)\Big|_{x=l} \right\|^2 = (\dot{\theta} + \dot{u}'(l,t))^2 + u'^2(l,t)\dot{\theta}^2. \tag{2.9}$$

To be able to use the cubic-spline spatial discretization technique, the kinetic and potential energies are reformulated in terms of time-varying displacement function at the nodal points along the beam and the angular velocity of the hub, namely,

$$T = T_1 + T_2 + T_3 + T_4 + T_5 + T_6 + T_h \tag{2.10}$$

(2.11)

$$V = \frac{1}{2}\sum_{k=1}^{n-1}\int_{x_k}^{x_{k+1}} EI_k\,[u''(x,t)]^2 dx \tag{2.12}$$

where

$$T_1 = \frac{1}{2}\dot{\theta}^2\sum_{k=1}^{n-1}\int_{x_k}^{x_{k+1}} \rho(x)s(x)u_k^2(x,t)dx \tag{2.13}$$

$$T_2 = \frac{1}{2}\sum_{k=1}^{n-1}\int_{r_k}^{r_{k+1}} \rho(r)s(r)\dot{u}_k^2(r,t)dr \tag{2.14}$$

$$T_3 = \dot{\theta}\sum_{k=1}^{n-1}\int_{r_k}^{r_{k+1}} \rho(r)s(r)u_k(r,t)r\,dr \tag{2.15}$$

$$T_4 = \frac{1}{2}\dot{\theta}^2\sum_{k=1}^{n-1}\int_{r_k}^{r_{k+1}} \rho(r)s(r)r^2dr \tag{2.16}$$

$$T_5 = \frac{1}{2}M[\,u^2(l,t)\theta^2 + l^2\dot{\theta}^2 + \dot{u}^2(l,t) + 2l\theta u(l,t)\,] \tag{2.17}$$

$$T_6 = \frac{1}{2}I_m[\,\dot{\theta}^2 + 2\dot{\theta}u'(l,t) + \dot{u}'^2(l,t) + u'^2(l,t)\theta^2\,] \tag{2.18}$$

$$T_h = \frac{1}{2}I_h\dot{\theta}^2 \tag{2.19}$$

2.2 Spatial Discretization and Consideration of Boundary Conditions Using Cubic Splines

The displacement function $u(x,t)$ in the interval $x_k \le x \le x_{k+1}$ is approximated by a cubic spline function as

$$u_k(x,t) = A_k(x-x_k)^3 + B_k(x-x_k)^2 + C_k(x-x_k) + D_k \tag{2.20}$$

where x_k is the abscissa of the kth nodal point of the spline (Späth 1978), and

$$A_k = \frac{1}{6\Delta x_k}(u''_{k+1} - u''_k) \tag{2.21}$$

$$B_k = \frac{1}{2}u''_k \tag{2.22}$$

$$C_k = \frac{\Delta u_k}{\Delta x_k} - \frac{1}{6}\Delta x_k(u''_{k+1} + 2u''_k) \tag{2.23}$$

$$D_k = u_k \tag{2.24}$$

where $\Delta x_k = x_{k+1} - x_k$ and $\Delta u_k = u_{k+1} - u_k$. Moreover, u_k and u''_k are, respectively, the displacement and the curvature at the kth nodal point.

When the moment of inertia of the tip mass is not considered, the governing partial differential equation and four boundary conditions of the given model are readily obtained by application of Hamilton's principle, namely,

$$EI(x)\frac{\partial^4 u}{\partial x^4} + m(x)\frac{\partial^2 u}{\partial t^2} = 0 \tag{2.25}$$

with the boundary conditions

$$\text{at } x = 0, \quad \begin{cases} u(x,t) = 0 \\ \frac{\partial u}{\partial x} = 0 \end{cases} \tag{2.26}$$

and

$$\text{at } x = l, \quad \begin{cases} EI(x)\frac{\partial^2 u}{\partial x^2} = 0 \\ EI(x)\frac{\partial^3 u}{\partial x^3} = M\frac{\partial^2 u}{\partial t^2} \end{cases} \tag{2.27}$$

where $m(x)$ is the mass of the beam per unit length at an arbitrary point and M is the tip mass. The geometric boundary condition $\partial u/\partial x = 0$ at the root of the beam then leads to

$$\left.\frac{\partial u}{\partial x}\right|_{x=0} \equiv u_1'(t) = 0 = \frac{1}{\Delta x_1}(u_2 - u_1) - \frac{1}{6}\Delta x_1(u_2'' + 2u_1'') \tag{2.28}$$

while the other geometric boundary condition, i.e. $u(0,t) = 0$ as given by eq. (2.26), gives

$$2\alpha_1 u_1'' + \alpha_1 u_2'' = 6\beta_1 u_2 \tag{2.29}$$

where $\alpha_k \equiv \Delta x_k$ and $\beta_k \equiv 1/\Delta_k$.

Furthermore, the presence of a kinetic boundary condition at the tip, which is expressed in terms of the shear force, can be considered by finding the end-point acceleration of the beam using the governing partial differential equation (Davis and Hirschorn 1988). This yields

$$M\frac{\partial^2 u}{\partial t^2}\bigg|_{x=l} = -\frac{EI(x)M}{m(x)}\left(\frac{\partial}{\partial x}\left(\frac{\partial^3 u}{\partial x^3}\right)\right)\bigg|_{x=l}. \tag{2.30}$$

The cubic-spline approximation provides a useful relation, namely,

$$u_n''' = \lambda_{n-1} = \beta_{n-1}(u_n'' - u_{n-1}''). \tag{2.31}$$

Hence, eq. (2.30) becomes

$$M\frac{\partial^2 u}{\partial t^2}\bigg|_{x=l} = -\frac{EI(l)\,M\beta_{n-1}}{m(l)}\frac{\partial}{\partial x}(u''_n - u''_{n-1}) \tag{2.32}$$

$$= -\frac{EI(l)M\beta_{n-1}^2}{m(l)}(u''_n - 2u''_{n-1} + u''_{n-2}) \tag{2.33}$$

Using the preceding results, the defined boundary condition, i.e., eq. (2.27), can be expressed as

$$EI(x)\frac{\partial^3 u}{\partial x^3}\bigg|_{x=l} = EI(l)(u''_n - u''_{n-1}) = -\frac{EI(l)\,M\beta_{n-1}^2}{m(l)}(u''_n - 2u''_{n-1} + u''_{n-2}) \tag{2.34}$$

and

$$u''_n = M_a u''_{n-1} - M_b u''_{n-2} \tag{2.35}$$

with M_a and M_b defined as

$$M_a = \frac{1 + 2(M\beta_{n-1}^2/m(l))}{1 + (M\beta_{n-1}^2/m(l))} \tag{2.36}$$

$$M_b = \frac{(M\beta_{n-1}^2/m(l))}{1 + (M\beta_{n-1}^2/m(l))}. \tag{2.37}$$

Furthermore, the continuity and smoothness conditions at the n nodal points yield the curvature-displacement relation, including the boundary conditions given by eqs. (2.29) and (2.35), as

$$\mathbf{A}_n\mathbf{u}'' = 6\mathbf{C}_n\mathbf{u} \tag{2.38}$$

where

$$\mathbf{A}_n = \begin{bmatrix} 2\alpha_1 & \alpha_1 & 0 & \cdots & 0 \\ \alpha_1 & 2\alpha'_1 & \alpha_2 & \cdots & 0 \\ 0 & \ddots & \ddots & \ddots & \vdots \\ 0 & \cdots & \alpha_{n-3} & 2\alpha'_{n-3} & \alpha_{n-2} \\ 0 & \cdots & 0 & \alpha_{n-2} - \alpha_{n-1}M_b & 2\alpha'_{n-2} + \alpha_{n-1}M_a \end{bmatrix} \in \mathbb{R}^{(n-1)\times(n-1)} \tag{2.39}$$

$$\mathbf{C}_n = \begin{bmatrix} \beta_1 & 0 & 0 & & & 0 \\ \beta'_1 & \beta_2 & 0 & \ddots & & \\ \beta_2 & -\beta'_2 & \beta_3 & 0 & & \\ 0 & \ddots & \ddots & \ddots & \ddots & \vdots \\ 0 & & 0 & \beta_{n-2} & -\beta'_{n-2} & \beta_{n'} \end{bmatrix} \in \Re^{(n-1)\times(n-1)} \tag{2.10}$$

$$\alpha_i \equiv \Delta x_i, \quad \beta_i \equiv 1/\Delta x_i, \quad \text{for } i = 1, \ldots, n-1$$

$$\alpha'_i \equiv \alpha_i + \alpha_{i+1}, \ \beta'_i \equiv \beta_i + \beta_{i+1}, \ \text{for } i = 1, \ldots, n-3$$

In eq (2.38), $\mathbf{u}$ is the vector of time-varying displacements and $\mathbf{u}''$ is the vector of time-varying curvature at the nodal points, given by

$$\mathbf{u} = \begin{bmatrix} u_2, \ldots, u_n \end{bmatrix}^T \in \Re^{(n-1)} \tag{2.11}$$

$$\mathbf{u}'' = \begin{bmatrix} u''_1, \ldots, u''_{n-1} \end{bmatrix}^T \in \Re^{(n-1)} \tag{2.12}$$

Thus, eq. (2.38) leads to

$$\mathbf{u} = \mathbf{N}\mathbf{u}'' \tag{2.13}$$

where

$$\mathbf{N} = \frac{1}{6}\mathbf{C}_n^{-1}\mathbf{A}_n \tag{2.14}$$

$\mathbf{C}_n$ being non singular.

The displacement function $u_k(x,t)$ can be expressed also as a function of $\mathbf{u}$ as shown below.

$$u_k(x,t) = \begin{bmatrix} (x-x_k)^3 & (x-x_k)^2 & (x-x_k) & 1 \end{bmatrix} \begin{bmatrix} A_k(t) \\ B_k(t) \\ C_k(t) \\ D_k(t) \end{bmatrix} \tag{2.15}$$

Defining $\mathbf{s}_k^I(x)$ as

$$\mathbf{s}_k^I(x) \equiv \begin{bmatrix} (x-x_k)^3 & (x-x_k)^2 & (x-x_k) & 1 \end{bmatrix}. \tag{2.16}$$

and substituting eqs. (2.21), (2.22), (2.23) and (2.24) into eq. (2.15) give

$$u_k(x,t) = \mathbf{s}_k^T(x) \begin{bmatrix} (u''_{k+1} - u''_k)/6\Delta x_k \\ u''_k/2 \\ (u_{k+1} - u_k)/\Delta x_k - (u''_{k+1} + 2u''_k)\Delta x_k/6 \\ u_k \end{bmatrix} \tag{2.17}$$

$$= \mathbf{s}_k^T(x) \begin{bmatrix} (u''_{k+1} - u''_k)/6\Delta x_k \\ u''_k/2 \\ -(u''_{k+1} + 2u''_k)\Delta x_k/6 \\ 0 \end{bmatrix} + \mathbf{s}_k^I(x) \begin{bmatrix} 0 \\ 0 \\ (u_{k+1} - u_k)/\Delta x_k \\ u_k \end{bmatrix} \tag{2.18}$$

which results in the relationship

$$u_k(x,t) = \mathbf{s}_k^T \mathbf{U}''_k \mathbf{u}'' + \mathbf{s}_k^I \mathbf{U}_k \mathbf{u}. \tag{2.19}$$

where $\mathbf{U}''_k$ is a $4 \times (n-1)$ matrix whose only non-zero entries appear in its $(k+1)$st and kth columns, namely,

$$\mathbf{U}''_k = \begin{bmatrix} 0 & \dots & 0 & -\beta_k/6 & \beta_k/6 & 0 & \dots & 0 \\ 0 & \dots & 0 & 1/2 & 0 & 0 & . & 0 \\ 0 & \dots & 0 & -\alpha_k/3 & -\alpha_k/6 & 0 & & 0 \\ 0 & \dots & 0 & 0 & 0 & 0 & \dots & 0 \end{bmatrix} \tag{2.20}$$

while $\mathbf{U}_k$ is a $4 \times (n-1)$ matrix whose only non-zero entries appear in its kth and $(k-1)$st columns, i.e.,

$$\mathbf{U}_k = \begin{bmatrix} 0 & .. & 0 & 0 & 0 & 0 & .. & 0 \\ 0 & . . & 0 & 0 & 0 & 0 & & 0 \\ 0 & \dots & 0 & -\beta_k & \beta_k & 0 & . & 0 \\ 0 & \dots & 0 & 1 & 0 & 0 & . & 0 \end{bmatrix}. \tag{2.21}$$

Finally, using eq. (2.13), the displacement function $u_I(x,t)$ becomes

$$u_k(x,t) = \mathbf{s}_k^I(\mathbf{U}''_k + \mathbf{U}_k \mathbf{N})\mathbf{u}'' \tag{2.22}$$

To express the potential energy as a function of the curvature vector, the cubic spline function defined in eq. (2.20) is used. Taking the second derivative of the displacement function $u(x,t)$ with respect to x, the curvature function $u''(x,t)$ is obtained, namely,

$$u_k'' = 6A_k(x - x_k) + 2B_k \tag{2.53}$$

$$= \begin{bmatrix} (x - x_k) & 1 \end{bmatrix} \begin{bmatrix} (u_{k+1}'' - u_k'')/\Delta x_k \\ u_k'' \end{bmatrix}. \tag{2.54}$$

Now, we define

$$\mathbf{t}_k^T(x) \equiv \begin{bmatrix} (x - x_k) & 1 \end{bmatrix} \tag{2.55}$$

which leads to

$$u_k'' = \mathbf{t}_k^T(x)\mathbf{F}''_k\mathbf{u}'' \tag{2.56}$$

where

$$\mathbf{F}''_k = \begin{bmatrix} 0 & \dots & 0 & -\beta_k & \beta_k & 0 & \dots & 0 \\ 0 & \dots & 0 & 1 & 0 & 0 & \dots & 0 \end{bmatrix}. \tag{2.57}$$

Note that $\mathbf{F}''_k$ is a $2 \times (n-1)$ matrix whose only non-zero entries appear in its $(k+1)$st and kth columns.

The kinetic and potential energy equations of the flexible beam can then be reformulated using eqs. (2.52) and (2.56), which allow the use of the cubic-spline technique, in terms of the curvature vector.

2.3 The Euler-Lagrange Equations of Motion

When the terms due to the centrifugal force are neglected, the kinetic and potential energy expressions are given by

$$T = \frac{1}{2}\left[I_t\dot{\theta}^2 + \dot{\mathbf{u}}''^T(\mathbf{M}''_1 + \mathbf{M}''_2 + \mathbf{M}''_3)\dot{\mathbf{u}}'' + 2\dot{\theta}(\boldsymbol{\gamma}_1^T + \boldsymbol{\gamma}_2^T + \boldsymbol{\gamma}_3^T)\dot{\mathbf{u}}'' \right] \tag{2.58}$$

$$V = \frac{1}{2}\mathbf{u}''^T\mathbf{K}''\mathbf{u}'' \tag{2.59}$$

where

$$I_t = I_b + I_b + I_m + Ml^2 \tag{2.60}$$

and the I_b is the moment of inertia of the unflexed rigid beam. Moreover,

$$\mathbf{M}''_1 = \sum_{k=1}^{n-1} (\mathbf{N}^T \mathbf{U}_k^T + \mathbf{U}''^T_k) \mathbf{P}_k (\mathbf{U}''_k + \mathbf{U}_k \mathbf{N}) \tag{2.61}$$

$$\mathbf{M}''_2 = (\mathbf{N}^T \mathbf{U}_{n-1}^T + \mathbf{U}''^T_{n-1}) \mathbf{P}_{n-1} (\mathbf{U}''_{n-1} + \mathbf{U}_{n-1} \mathbf{N}) \tag{2.62}$$

$$\mathbf{M}''_3 = (\mathbf{N}^T \mathbf{U}_{n-1}^T + \mathbf{U}''^T_{n-1}) \mathbf{P}'_{n-1} (\mathbf{U}''_{n-1} + \mathbf{U}_{n-1} \mathbf{N}) \tag{2.63}$$

where $\mathbf{P}_k$, $\mathbf{P}_{n-1}$ and $\mathbf{P}'_{n-1}$ are 1×1 matrices, the first one being positive-definite, the others positive-semidefinite, namely,

$$\mathbf{P}_k = \int_{x_k}^{x_{k+1}} \rho_k s_k \, \mathbf{s}_k(x) \, \mathbf{s}_k^T(x) \, dx \tag{2.64}$$

$$\mathbf{P}_{n-1} = M \, \mathbf{s}_{n-1}(l) \, \mathbf{s}_{n-1}^T(l) \tag{2.65}$$

$$\mathbf{P}'_{n-1} = I_m \, \mathbf{s}'_{n-1}(l) \, \mathbf{s}'^T_{n-1}(l) \tag{2.66}$$

where $\mathbf{s}'_{n-1}(l)$ denotes the derivative $\mathbf{s}'_{n-1}(x)$ evaluated at $x = l$. The $\boldsymbol{\gamma}_1^T$, $\boldsymbol{\gamma}_2^T$ and $\boldsymbol{\gamma}_3^T$ are also derived from eqs. (2.15), (2.17), (2.18) and eq. (2.52), which yield

$$\boldsymbol{\gamma}_1^T = \sum_{k=1}^{n-1} \mathbf{m}''^T_k + \left(\sum_{k=1}^{n-1} \mathbf{m}_k^T \right) \mathbf{N} \tag{2.67}$$

$$\boldsymbol{\gamma}_2^T = \mathbf{m}''^T_{n-1} + \mathbf{m}_{n-1}^T \mathbf{N} \tag{2.68}$$

$$\boldsymbol{\gamma}_3^T = \hat{\mathbf{m}}''^T_{n-1} + \hat{\mathbf{m}}_{n-1}^T \mathbf{N} \tag{2.69}$$

where

$$\mathbf{m}''^T_k \equiv \mathbf{p}_k^T \mathbf{U}''_k \qquad \mathbf{m}_k^T \equiv \mathbf{p}_k^T \mathbf{U}_k \tag{2.70}$$

$$\mathbf{m}''^T_{n-1} \equiv \mathbf{p}_{n-1}^T \mathbf{U}''_{n-1} \qquad \mathbf{m}_{n-1}^T \equiv \mathbf{p}_{n-1}^T \mathbf{U}_{n-1} \tag{2.71}$$

$$\hat{\mathbf{m}}''^T_{n-1} \equiv \mathbf{p}'^T_{n-1} \mathbf{U}''_{n-1} \qquad \hat{\mathbf{m}}_{n-1}^T \equiv \mathbf{p}'^T_{n-1} \mathbf{U}_{n-1} \tag{2.72}$$

with

$$\mathbf{p}_k^T = \int_{x_k}^{x_{k+1}} \rho_k \, s_k \, x \, \mathbf{s}_k^T(x) dx \tag{2.73}$$

$$\mathbf{p}^{I}_{n-1} = M\ I\ \mathbf{s}^{I}_{n-1}(l) \tag{2.74}$$

$$\mathbf{p}'^{I}_{n-1} = I_m\ I\ \mathbf{s}'^{I}_{n-1}(l). \tag{2.75}$$

The positive definite stiffness matrix $\mathbf{K}$ is defined as

$$\mathbf{K} = \sum_{k=1}^{n-1} \mathbf{F}''^{I}_{k}\, \mathbf{Q}_k \mathbf{F}''_k \tag{2.76}$$

with

$$\mathbf{Q}_k = \int_{x_k}^{l_{k+1}} EI_k\ \mathbf{t}_k(x)\, \mathbf{t}_k^{T}(x)\, dx \in \Re^{(2\times 2)} \tag{2.77}$$

where $\mathbf{Q}_k$ is positive definite.

The kinetic and potential energy expressions can be simplified using the Euler-Lagrange equation as

$$T = \frac{1}{2}\dot{\mathbf{q}}^T \mathbf{M}\dot{\mathbf{q}},\quad V = \frac{1}{2}\mathbf{q}^T \mathbf{K}\mathbf{q} \tag{2.78}$$

where

$$\mathbf{M} = \begin{bmatrix} \mathbf{M}'' & \boldsymbol{\gamma} \\ \boldsymbol{\gamma}^T & I_t \end{bmatrix},\quad \mathbf{K} = \begin{bmatrix} \mathbf{K}'' & \mathbf{0}_{n\times 1} \\ \mathbf{0}_{1\times n} & 0 \end{bmatrix} \tag{2.79}$$

are the mass and stiffness matrices, with

$$\mathbf{M}'' \equiv \mathbf{M}''_1 + \mathbf{M}''_2 + \mathbf{M}''_3 \tag{2.80}$$

$$\boldsymbol{\gamma} \equiv \boldsymbol{\gamma}_1 + \boldsymbol{\gamma}_2 + \boldsymbol{\gamma}_3, \tag{2.81}$$

while the vector of generalized coordinates is defined as

$$\mathbf{q} = [\ \mathbf{u}''^{T}\ \ \theta\ ]^T. \tag{2.82}$$

Finally, the equation of motion of the beam is obtained as

$$\mathbf{M}\ddot{\mathbf{q}} + \mathbf{K}\mathbf{q} = \boldsymbol{\varphi}(t) \tag{2.83}$$

where

$$\boldsymbol{\varphi}(t) = [\ \mathbf{0}^{T}_{(n-1)}\ \ \tau(t)\ ]^T \tag{2.84}$$

in which $\tau(t)$ is the applied torque and $\mathbf{0}_{(n-1)}$ is the $(n-1)$-dimensional zero vector.

In order to reduce the model given by eq. (2.83) to one in which the coefficient of the term containing the second derivative is the identity matrix and the coefficient of $\mathbf{q}$ is symmetric, the Cholesky decomposition (Dahlquist and Björck 1971) of $\mathbf{M}$ is performed. Since $\mathbf{M}$ is positive definite, it can be factored as $\mathbf{M} = \mathbf{L}^T\mathbf{L}$, where $\mathbf{L}$ is lower triangular. Premultiplying both sides of eq. (2.83) by $\mathbf{L}^{-T}$, the transpose of $\mathbf{L}^{-1}$, gives

$$\mathbf{L}\ddot{\mathbf{q}} + \mathbf{L}^{-T}\mathbf{K}\mathbf{q} = \mathbf{L}^{-T}\boldsymbol{\varphi}. \tag{2.85}$$

Letting $\mathbf{v} \equiv \mathbf{L}\mathbf{q}$, the mathematical model given by eq. (2.83) reduces to

$$\ddot{\mathbf{v}} + \mathbf{W}\mathbf{v} = \boldsymbol{\psi} \tag{2.86}$$

where the new mass stiffness matrix $\mathbf{W}$ and the new generalized force vector $\boldsymbol{\psi}$ are defined as

$$\mathbf{W} \equiv \mathbf{L}^{-T}\mathbf{K}\mathbf{L}^{-1}, \quad \boldsymbol{\psi} \equiv \mathbf{L}^{-1}\boldsymbol{\varphi} \tag{2.87}$$

in which $\mathbf{W}$ is also positive definite.

Chapter 3

Optimal Control System Design

The design of a controller for the flexible beam must take into consideration the presence of uncertain and time-varying parameters due to imperfect modelling of system dynamics, as well as the presence of noise due to the imperfection of strain gages used for measurements. Therefore, an optimal control approach is chosen to minimize these effects and to aid in the determination of the desired pole location. The optimal control strategy is two-fold: one is the design of the Kalman filter, which minimizes the variance of state estimation errors, while the other is the determination of the optimal control law to minimize the specified performance criterion from the estimated states.

3.1 State-Space Model Description

The Lagrangian model of the flexible beam can be described as a continuous-time, linear, constant-coefficient system in state-variable space, namely,

$$\dot{\mathbf{x}} = \mathbf{A}\mathbf{x}(t) + \mathbf{b}u(t), \quad \mathbf{x}(0) = \mathbf{x}_0 \tag{3.1}$$

$$\mathbf{y} = \mathbf{C}\mathbf{x}(t) \tag{3.2}$$

where

$$\mathbf{A} = \begin{bmatrix} \mathbf{O} & \mathbf{1} \\ -\mathbf{W} & \mathbf{O} \end{bmatrix} \in \Re^{(2n \times 2n)} \tag{3.3}$$

$$\mathbf{b} = \begin{bmatrix} \mathbf{0} \\ \mathbf{L}^{-1}\mathbf{w} \end{bmatrix} \in \Re^{2n}, \quad \mathbf{w} = \begin{bmatrix} \mathbf{0}_{(n-1)} \\ 1 \end{bmatrix}, \quad \mathbf{C} \in \Re^{(p \times 2n)} \tag{3.4}$$

in which $\mathbf{O}$ and $\mathbf{1}$ denote the $n \times n$ zero and identity matrices, respectively. Moreover, $\mathbf{0}$ is the n-dimensional zero vector, $\mathbf{0}_{(n-1)}$ is the $(n-1)$-dimensional zero vector, and p denotes the number of sensors. The state vector and scalar input are also defined as

$$\mathbf{x} = \begin{bmatrix} \mathbf{v} \\ \dot{\mathbf{v}} \end{bmatrix}, \quad u(t) = \tau(t). \tag{3.5}$$

It is impractical to assume that all of the state variables are available through measurement. For instance, the state variables associated with the time rate of change of curvature cannot be measured directly with any existing sensor. Furthermore, the use of a large number of sensors would require more complicated control hardware having a high data throughput capability. The approach adopted here is to measure a subset of the state variables and to estimate on-line the remaining ones. Therefore, the measured output through p sensors is expressed as a linear combination of the available state variables, i.e.

$$\mathbf{y} = \mathbf{C}' \begin{bmatrix} \mathbf{q} \\ \dot{\mathbf{q}} \end{bmatrix} \tag{3.6}$$

where $\mathbf{C}' \equiv \mathbf{CL} \in \Re^{(p \times 2n)}$.

A digital control signal is assumed to be applied via a zero-order hold, the associated discrete-time system being the step-invariant model given by

$$\mathbf{x}(k+1) = \mathbf{\Phi}\mathbf{x}(k) + \mathbf{\Gamma}u(k) + \boldsymbol{\omega}(k) \tag{3.7}$$

$$\mathbf{y}(k) = \mathbf{H}\mathbf{x}(k) + \boldsymbol{\upsilon}(k) \tag{3.8}$$

where

$$\mathbf{\Phi} = e^{\mathbf{A}\Delta} \tag{3.9}$$

$$\mathbf{\Gamma} = \left(\int_0^{\Delta} e^{\mathbf{A}\eta} d\eta \right) \mathbf{b} \tag{3.10}$$

$$\mathbf{H} = \mathbf{C} \tag{3.11}$$

and the process noise $\boldsymbol{\omega}(k)$ and measurement noise $\boldsymbol{v}(k)$ are random, uncorrelated processes with zero mean value and the diagonal variance matrices given, respectively, by

$$E\{\boldsymbol{\omega}(k)\boldsymbol{\omega}(k)^T\} = \mathbf{R}_v, \quad E\{\boldsymbol{v}(k)\boldsymbol{v}(k)^T\} = \mathbf{R}_r. \tag{3.12}$$

In the foregoing equations, Δ is the sampling time interval, and k represents the kth sampling time step.

3.2 Optimal Observer

Let the state observer be given by

$$\hat{\mathbf{x}}(k+1) = \boldsymbol{\Phi}\hat{\mathbf{x}}(k) + \boldsymbol{\Gamma}u(k) + \mathbf{L}_\infty[\mathbf{y}(k) - \mathbf{H}\hat{\mathbf{x}}(k)] \tag{3.13}$$

where $\mathbf{L}_\infty$ is the steady-state, discrete-time, Kalman filter gain matrix. It is well known (Middleton and Goodwin 1990) that if the pair $(\mathbf{H}, \boldsymbol{\Phi})$ is observable, the eigenvalues of $(\boldsymbol{\Phi} - \mathbf{L}_\infty\mathbf{H})$ can be arbitrarily assigned by appropriate design of the steady-state gain matrix, $\mathbf{L}_\infty$. It is also known (Luenberger 1971) that the observer does not impair the closed loop stability. Therefore, the design of an optimal observer reduces to optimization of the steady-state observer gain matrix $\mathbf{L}_\infty$ so as to minimize the estimation error $\tilde{\mathbf{x}} = \mathbf{x} - \hat{\mathbf{x}}$ governed by

$$\tilde{\mathbf{x}}(k+1) = [\boldsymbol{\Phi} - \mathbf{L}_\infty\mathbf{H}]\tilde{\mathbf{x}}(k) + \boldsymbol{\omega}(k) - \mathbf{L}_\infty\boldsymbol{v}(k). \tag{3.14}$$

To find the steady-state, discrete-time, Kalman filter gain $\mathbf{L}_\infty$ (current observer gain), the parametric optimization problem associated with the covariance of the estimation error (Åström and Wittenmark 1984; Franklin, Powell and Workman 1990) is solved in the presence of noise.

3.3 Optimal Controller

The reference state $\mathbf{x}_r$ is derived from the reference input r through the relation

$$\mathbf{x}_r(k) = \mathbf{T}_r r(k) \tag{3.15}$$

where $\mathbf{T}_r$ is the constant state command matrix which is determined so that

$$\lim_{k\to\infty} \mathbf{x}_r(k) = \mathbf{x}_{ss}(k) \tag{3.16}$$

in which $\mathbf{x}_{ss}(k)$ is the steady-state response of the unit step.

The control input is then generated by

$$u(k) = -\mathbf{k}_\infty^T(\hat{\mathbf{x}}(k) - \mathbf{x}_r(k)) \tag{3.17}$$

where $\hat{\mathbf{x}}$ is the estimated state-vector and $\mathbf{k}_\infty$ is the steady-state, discrete-time controller gain, which minimizes the cost function given by

$$J = \frac{1}{2}\sum_{k=0}^{N}[\mathbf{x}^T(k)\mathbf{Q}\mathbf{x}(k) + qu^2(k)] \tag{3.18}$$

under the constraint

$$-\mathbf{x}(k+1) + \mathbf{\Phi}\mathbf{x}(k) + \mathbf{\Gamma}u(k) = 0, \quad k = 0, 1, \quad \ldots N. \tag{3.19}$$

It should be noted that $\mathbf{Q}$ is symmetric and positive semidefinite and q is positive definite.

Because of its numerical simplicity and reliability, the eigenvalue-decomposition method associated with the Hamiltonian matrix is used to find the optimal steady state control gain $\mathbf{k}_\infty$, instead of solving the discrete algebraic Riccati equation, which can have multiple solutions. The Hamilton equations are:

$$\begin{bmatrix} \mathbf{x} \\ \boldsymbol{\lambda} \end{bmatrix}_{k+1} = \begin{bmatrix} \mathbf{\Phi} + \mathbf{\Gamma}\mathbf{Q}^{-1}\mathbf{\Gamma}^T\mathbf{\Phi}^{-T}q & -\mathbf{\Gamma}r^{-1}\mathbf{\Gamma}^T\mathbf{\Phi}^{-T} \\ -\mathbf{\Phi}^{-T}\mathbf{Q} & \mathbf{\Phi}^{-T} \end{bmatrix} \begin{bmatrix} \mathbf{x} \\ \boldsymbol{\lambda} \end{bmatrix}_k \tag{3.20}$$

where the $\boldsymbol{\lambda}$ is a discrete-time Lagrange multiplier and $\mathbf{\Phi}$ is invertible by definition, eq. (3.9). The optimal control gain $\mathbf{k}_\infty$ can be calculated by determining the eigenvalues of the Hamiltonian matrix.

3.4 Combined Optimal Controller and Observer

The control strategy used in this study is a combination of the state variable feedback controller and the optimal state observer. Thus, an estimate of the state vector $\hat{\mathbf{x}}$ is obtained

using the Kalman filter, namely,

$$\hat{\mathbf{x}}(k) = [\mathbf{\Phi} - \mathbf{\Gamma}\mathbf{k}_{\sim}^{T} - \mathbf{L}_{\sim}\mathbf{H}]\hat{\mathbf{x}}(k-1) + \mathbf{L}_{\sim}\mathbf{y}(k-1) \tag{3.21}$$

Because the use of $\hat{\mathbf{x}}$, instead of $\mathbf{x}$, does not affect the control gain according to separation property (Kailath 1980), it is natural to apply the optimal feedback gain $\mathbf{k}_{\sim}$ to the estimated state vector $\hat{\mathbf{x}}$, that is

$$u(k) = -\mathbf{k}_{\sim}^{T}[\hat{\mathbf{x}}(k) - \mathbf{x}_{r}(k)]. \tag{3.22}$$

Therefore, the model of the overall system becomes

$$\mathbf{x}(k+1) = \mathbf{\Phi}\mathbf{x}(k) - \mathbf{\Gamma}\mathbf{k}_{\sim}^{T}[\hat{\mathbf{x}}(k) - \mathbf{x}_{r}(k)] \tag{3.23}$$

which is shown in Figure 3.1 in block-diagram form.

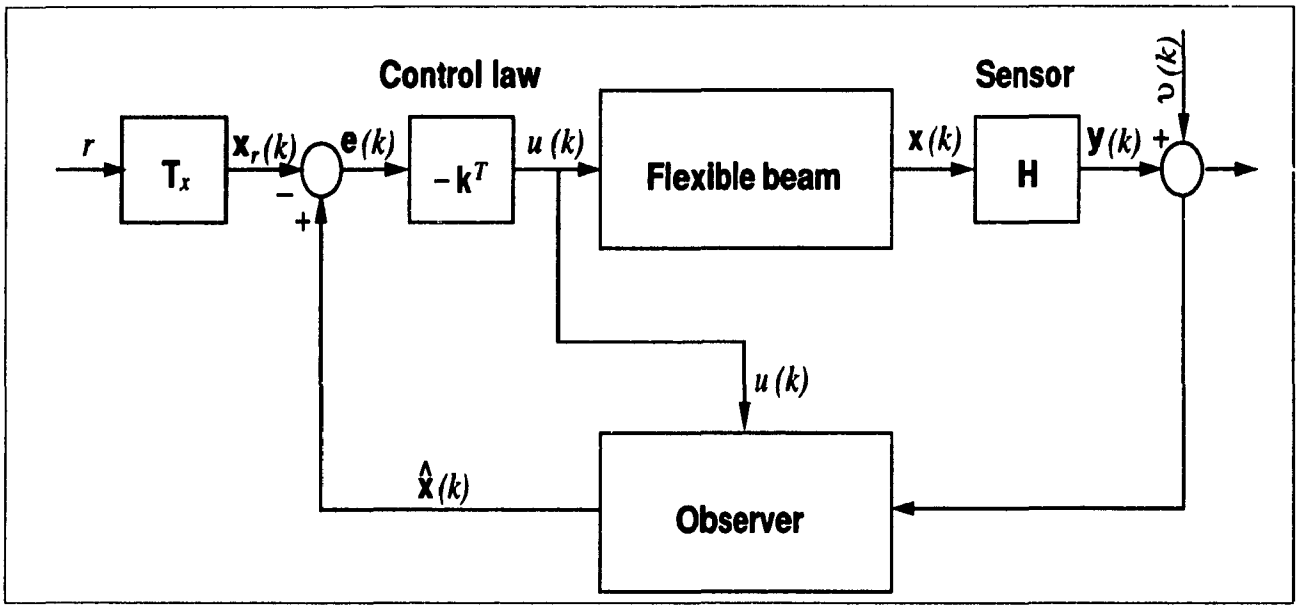

Figure 3.1: Combination of observer and controller

Chapter 4

Simulation of Flexible Beams Under Large Rigid-Body Motion

Sensing considerations are essential to a successful real-time implementation of the proposed control scheme. These considerations include the selection of the sampling rate and the determination of the number and location of sensors (which are actually the number and location of the nodal points of the approximating cubic spline).

The cubic-spline technique and optimal control scheme described in Chapters 2 and 3 will be applied to the modelling and simulation of the flexible beam. The controller is designed to suppress the transverse vibrations while forcing the end tip to follow the prescribed trajectory. State-observability and controllability problems associated with the reduced number of measurements are investigated through simulation studies in two cases, i.e., with and without tip mass for purposes of comparison. In addition, an investigation is conducted to demonstrate the dynamic effects of link flexibility by applying an optimal torque input, computed for a closed-loop system of an equivalent rigid beam, to the flexible beam in open-loop.

Table 4.1: The occurrence of maximum curvature [m^{-1}] for each of the low vibration mode

no	location in m	the 1st mode	the 2nd mode	the 3rd mode	the 4th mode
1	0.0	**2.0**	**2.0**	**2.0**	**2.0**
2	0.22	1.39660	-0.02865	-0.96375	**-1.32262**
3	0.30	1.18175	-0.63110	**-1.31485**	-0.79478
4	0.50	0.67905	-1.12733	0.03937	**1.41424**
5	0.52	0.63321	**-1.43920**	0.26103	1.37836
6	0.72	0.21030	-0.96827	**1.51056**	-1.10616
7	0.80	0.12774	-0.60211	1.20901	**-1.50758**

4.1 Number and Location of Sensors

Normally, the accuracy of the approximation of the spatial discretization of the continuous beam improves with an increase in the number of nodal points; however, a large number of nodal points can produces a large system of equations, thereby making the on-line control unfeasible. Thus, the proper selection of the number of sensors is a compromise between the accuracy of the approximation and the feasibility of on-line implementation. Furthermore, the positioning of the sensors can strongly affect the dynamic performance of the system and must be considered in both the plant-modelling and design of the control system. Guidelines for the minimum number of sensors required for satisfactory performance have stated that the number must be at least as large as the number of monitored vibration modes (Barsh and Choe 1989), which is in fact the number of generalized coordinates in the system represented eq. (2.83).

However, a different approach for choosing the number and location of sensors is taken. First, it is to be noted that the i^{th} vibrational mode has i points at which the bending moment reaches a maximum. In addition, simulation results, some of which are presented later in this thesis, have shown that locating a sensor at the position of maximum bending moment provides the most accurate estimation. This is because this location yields the highest signal

Table 1.2: The number and location of sensors

no. of sensors	location in m	maximum curvature [m^{-1}]
1	0.0	2.0
2	0.22	-1.32262
3	0.30	-1.31485
4	0.52	-1.13920
5	0.72	1.51056
6	0.80	-1.50758

to noise ratio, thus allowing the most accurate reconstruction of the remaining states. Thus, the approach adopted in this thesis is to locate a sensor at each point of maximum bending moment for all the modes to be controlled. Thus, once the number of vibration modes to be controlled is specified, the number of sensors as well as their location are readily determined. It should be realized, however, that the location of maximum bending moment for different vibrational modes may be in fact so close together as to prevent the mounting of individual sensors (no. 4 and 5 in Table 1.1). In this case, only one sensor will be used for both points.

In this thesis, the fourth mode of vibration is specified as the highest mode to be controlled, which is consistent with the work of (Hughes 1987), who has stated that, for practical purposes, only the lower vibrational modes are important for vibrational control. The location of the points of maximum bending moment for all modes up to the fourth, for the beam under consideration, have been obtained using a normal mode analysis for a clamped free beam without a tip mass (Bishop 1960), and are shown in Table 1.1. In addition, the selected number and location of the sensors are shown in Table 1.2. It is important to realize that only a subset of all the sensors will actually be physically realized in the control hardware, the Kalman filter being used to estimate the values for the remaining sensors, as described in greater detail in Section 1.3.

4.2 Selection of the Sampling Rate

The selection of the sampling rate guaranteeing adequate performance of the digital control scheme is essential in the implementation of the continuous-time system by a digital computer. A slower sampling rate leads to a loss of control information associated with inter-sampling behavior, resulting in poor control performance. An excessively fast sampling rate gives numerical difficulties and requires more advanced control and high precision computational hardware. Hence, the tradeoffs must be carefully examined. Moreover, high frequency resonances presented in this flexible beam that are faster than closed-loop system bandwidth must be considered for the selection of appropriate sampling rate.

The natural or resonance frequencies of the open-loop system model are found by using the equations of motion given in Chapter 2. The equation of motion obtained from the Euler-Lagrange formulation was given as

$$\mathbf{M}\ddot{\mathbf{q}} + \mathbf{K}\mathbf{q} = \boldsymbol{\varphi}(t) \tag{4.1}$$

where

$$\mathbf{M} = \begin{bmatrix} \mathbf{M}'' & \boldsymbol{\gamma} \\ \boldsymbol{\gamma}^T & I_t \end{bmatrix}, \quad \mathbf{K} = \begin{bmatrix} \mathbf{K}'' & \mathbf{0}_{n\times 1} \\ \mathbf{0}_{1\times n} & 0 \end{bmatrix} \tag{4.2}$$

$$\boldsymbol{\varphi}(t) = [\,\mathbf{0}^T \;\; \tau(t)\,]^T, \tag{4.3}$$

while $\tau(t)$ is the applied torque and $\mathbf{0}$ is the $(n-1)$-dimensional zero vector. Moreover, the matrices $\mathbf{M}''$ and $\mathbf{K}''$, the vector $\boldsymbol{\gamma}$, and the scalar I_t specific to this example are given as

$$\mathbf{M}'' = \begin{bmatrix} 0.0220247 & 0.0282172 & 0.0251101 & 0.0311296 & 0.0111284 & 0.079243 \\ 0.0282172 & 0.0363372 & 0.0326511 & 0.0408893 & 0.0191239 & 0.106238 \\ 0.0251101 & 0.0326511 & 0.0298962 & 0.0381850 & 0.0181686 & 0.103083 \\ 0.0311296 & 0.0408893 & 0.0381850 & 0.0198267 & 0.0211502 & 0.110069 \\ 0.0111281 & 0.0191239 & 0.0181686 & 0.0211502 & 0.0118938 & 0.070285 \\ 0.0792130 & 0.1062380 & 0.1030830 & 0.1100690 & 0.0702851 & 0.125007 \end{bmatrix} \text{kg m}^4$$

$$K'' = \begin{bmatrix} 1.1715 & 0.585751 & 0 & 0 & 0 & 0 \\ 0.585751 & 1.5975 & 0.213 & 0 & 0 & 0 \\ 0 & 0.213 & 1.5975 & 0.585751 & 0 & 0 \\ 0 & 0 & 0.585751 & 2.2365 & 0.5325 & 0 \\ 0 & 0 & 0 & 0.5325 & 1.191 & 0.213 \\ 0 & 0 & 0 & 0 & 0.213 & 3.621 \end{bmatrix} \text{N m}^{-1}$$

$$\gamma = \begin{bmatrix} 0.209129 \\ 0.266991 \\ 0.236052 \\ 0.290621 \\ 0.133861 \\ 0.72929 \end{bmatrix} \text{kg m}^{-1}\text{s}$$

$$I_t = 1.99135 \text{ kg m}^2.$$

The calculated resonance frequencies of the open-loop system with and without a tip mass are given in Table 1.3.

Table 1.3: The calculated natural vibration frequencies

Mode Number	the 1^{st}	the 2^{nd}	the 3^{rd}	the 4^{th}	the 5^{th}	the 6^{th}
Frequency with mass (Hz)	0.7309	11.7831	10.9813	80.5961	138.1216	208.9190
Frequency without mass (Hz)	9.1581	20.9435	18.2876	87.1222	150.1857	231.8915

If the system having high resonance frequencies is lightly damped and the controller introduces additional damping to those modes which are faster than the bandwidth of the system at hand, sensitive sampling rates related to the resonant frequencies of the system exist. The plant considered in this thesis contains high-frequency system dynamics with

very light structural damping and, thus, the order of magnitude of the closed-loop system bandwidth is much lower than the open-loop system resonances. In addition, the controller adds damping to the system resonances, when nearly collocated sensors and actuator are used. Thus, the digital controller using a sampling rate chosen according to the closed-loop bandwidth criterion may introduce unacceptable sensitivities to plant disturbances, making it impossible to obtain adequate control performance (Franklin et al. 1990). This is because if the sampling rate selected according to the closed-loop bandwidth of the system is less than twice an important open loop system resonance, the controlled system may be more sensitive to errors. Therefore, a relatively high sampling rate of 500 Hz is chosen, assuming that the highest open-loop system resonance to be controlled is the fourth natural vibration mode.

4.3 Observability Considerations

It is often not practical to assume that the entire state vector is available through measurements. In this thesis, an investigation is conducted to assess the possibility of a reduced number of measurements taken at a selected number of nodal points. The Kalman filter is used to optimally estimate the curvature at the other points as well as its time rate of change. Whether we will be able to use partial measurements depends upon the state-observability and controllability of the system. In principle, one may prove state-observability and controllability by showing that the associated observability and controllability matrices are each of full rank. The observability and controllability has already been studied by Balas (1978) and Hughes and Skelton (1980). It has also been shown that a system having only one sensor makes the system both state-controllable and observable. However, the numerical ill-conditioning of the associated controllability and observability matrices can prevent the Kalman filter from reconstructing the state estimates to a reasonable accuracy, especially when there is a tip mass, making the system unobservable for practical purposes.

It is desirable to assess the numerical viability of the state estimation using a reduced number of measurements. In addition, it is also beneficial to investigate the effectiveness of

Table 1.1: The curvature and associated first time derivative for an initial end point displacement of the beam

nodal point	r [m]	u'' [m^{-1}]	$\dot{u}''$ [$m^{-1}s^{-1}$]
1	0.0	2.0	0
2	0.22	1.39660	0
3	0.30	1.18175	0
4	0.52	0.67905	0
5	0.72	0.24030	0
6	0.80	0.12774	0

locating the sensors at the points of maximum bending moment.

This shall be done by analyzing the response of the beam to an initial end-point displacement with the hub fixed and without control input. Both cases, with and without tip mass, shall be analyzed. The initial conditions are listed in Table 1.1. The results of Kalman filtering for both cases are shown in Fig. 1.1 and Fig. 1.2, respectively. For the no mass on the tip case with two measurements, i.e., the curvature at the root of the beam and the hub rotational angle, the Kalman filter software succeeds in allocating the optimal steady-state gain matrix shown in Fig. 1.1. However, with tip mass, the simulation results show that the Kalman filter fails to find the steady-state observer gain matrix; that is, the system, although mathematically observable, is not observable in a practical sense due to roundoff errors. Nevertheless, state estimation of the flexible beam with tip mass can be accomplished if at least three measurements are taken, these being the curvatures at the the first and second nodal points, as well as the hub rotational angle. Fig. 1.2 shows the time history of a typical estimation error for this case. It has been found that the placing the sensors at the maximum bending moment points, including the root of the beam, which corresponds to a maximum bending moment for all vibration modes, gives good estimation results.

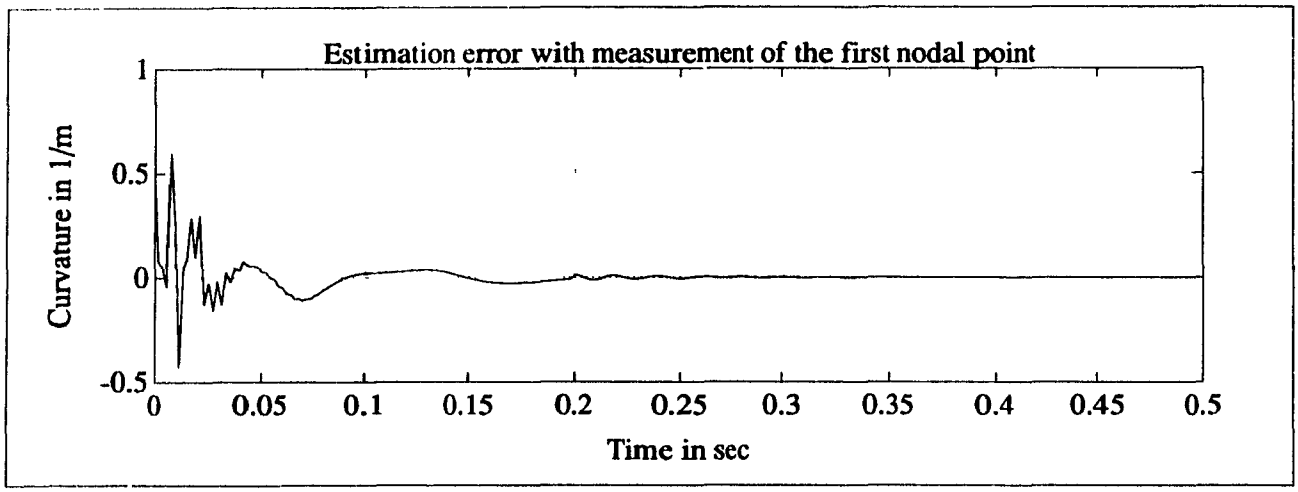

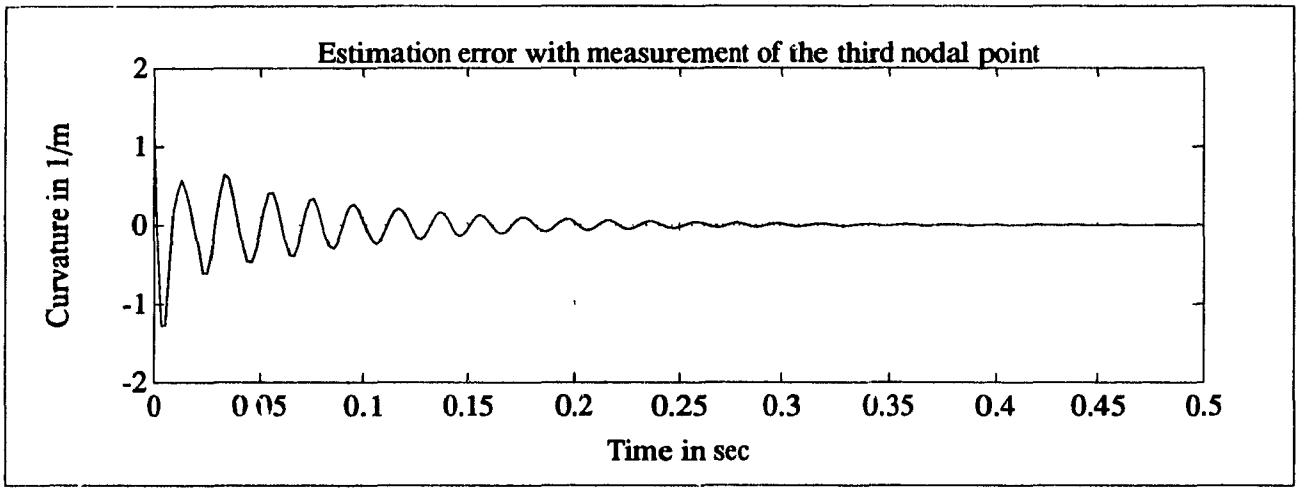

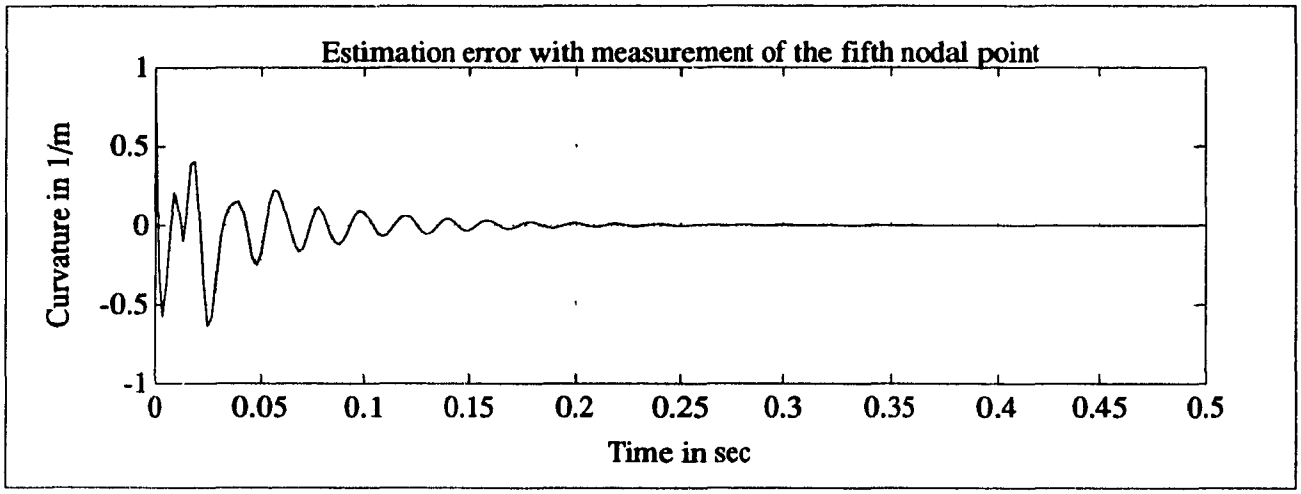

Figure 1.1: Estimation error of the state variables at the first nodal point without tip mass

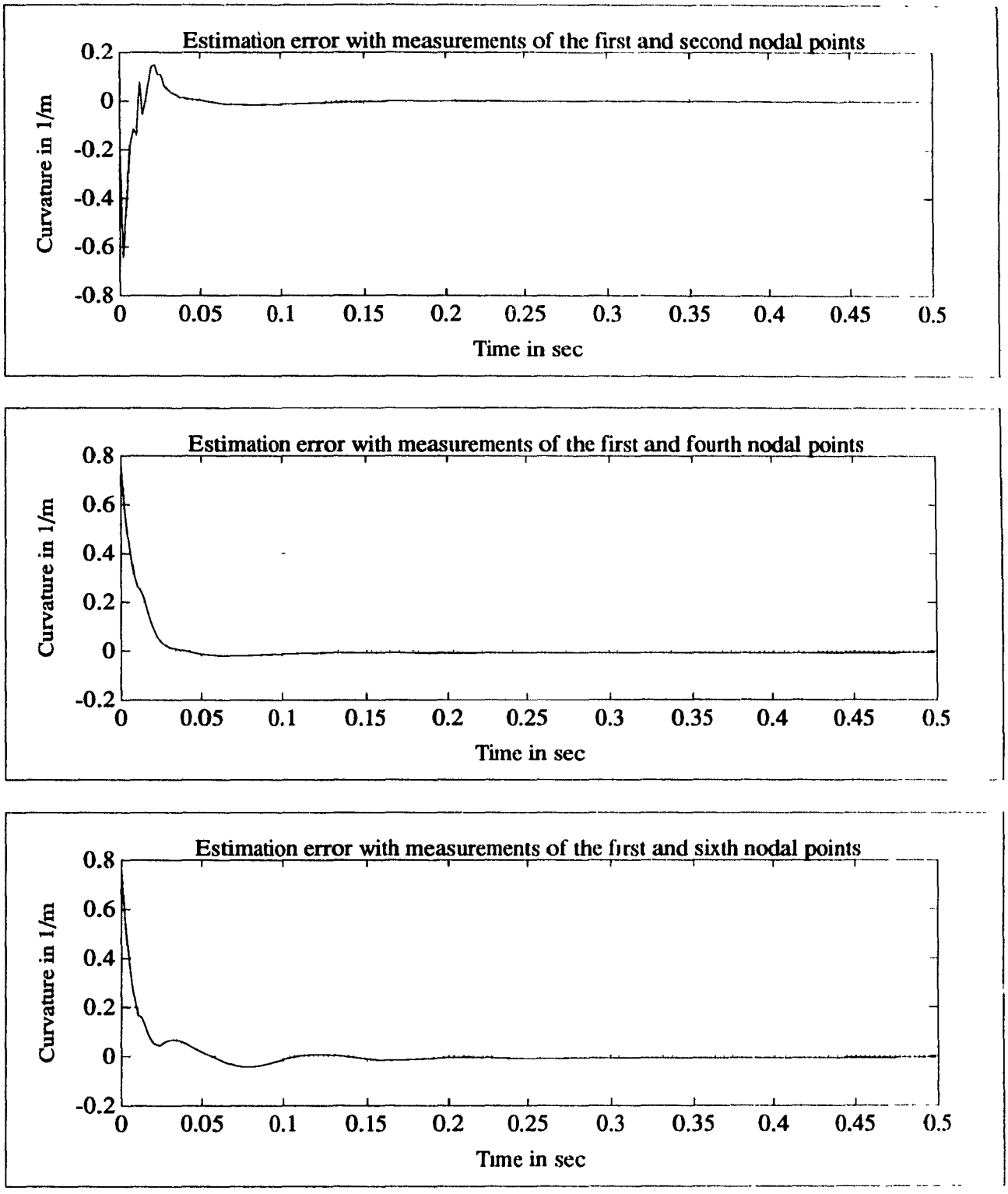

Figure 1.2: Estimation error of the state variables at the first nodal point with tip mass

4.4 Uncontrolled Vibrating Beam

If the lateral curvature component u'' is constrained to be zero in the system represented by eq (2.81) in Chapter 2, the equation of motion of non-flexible beam is obtained as

$$I_t \ddot{\theta} = \tau(t) \tag{4.4}$$

This can be described as a continuous-time, linear, constant-coefficient system in state-variable space, namely,

$$\dot{\mathbf{z}}(t) = \mathbf{A}_t \mathbf{z}(t) + \mathbf{b}_t u(t), \quad \mathbf{z}(0) = \mathbf{z}_0 \tag{4.5}$$

$$\mathbf{y}(t) = \mathbf{c}^T \mathbf{z}(t). \tag{4.6}$$

where

$$\mathbf{A}_t = \begin{bmatrix} 0 & 1 \\ 0 & 0 \end{bmatrix} \in \Re^{(2\times 2)} \tag{4.7}$$

$$\mathbf{b}_t = \begin{bmatrix} 0 \\ 1/I_t \end{bmatrix} \in \Re^2, \quad \mathbf{c}^T \in \Re^2. \tag{4.8}$$

The state vector and scalar input are also defined as

$$\mathbf{z} = \begin{bmatrix} \theta \\ \dot{\theta} \end{bmatrix}, \quad u(t) = \tau(t). \tag{4.9}$$

In order to find the computed torque input of this non-flexible beam, the associated step-invariant, discrete-time model is used. The computed torque of the non-flexible beam for a step input of hub rotational angle is readily obtained by employing the Kalman filter and is applied to the open-loop system of the flexible beam. This is performed for both cases with and without a tip mass. The computed torques and their time responses of the non-flexible system are shown in Figs. 4.3 and 4.5. The time responses of the flexible beam obtained by applying the same computed torque inputs of the non-flexible beams are also shown in Figs. 4.4 and 4.6. These show that large oscillations in the responses of the hub rotational angle and node displacements are attributed to the neglected link flexibility.

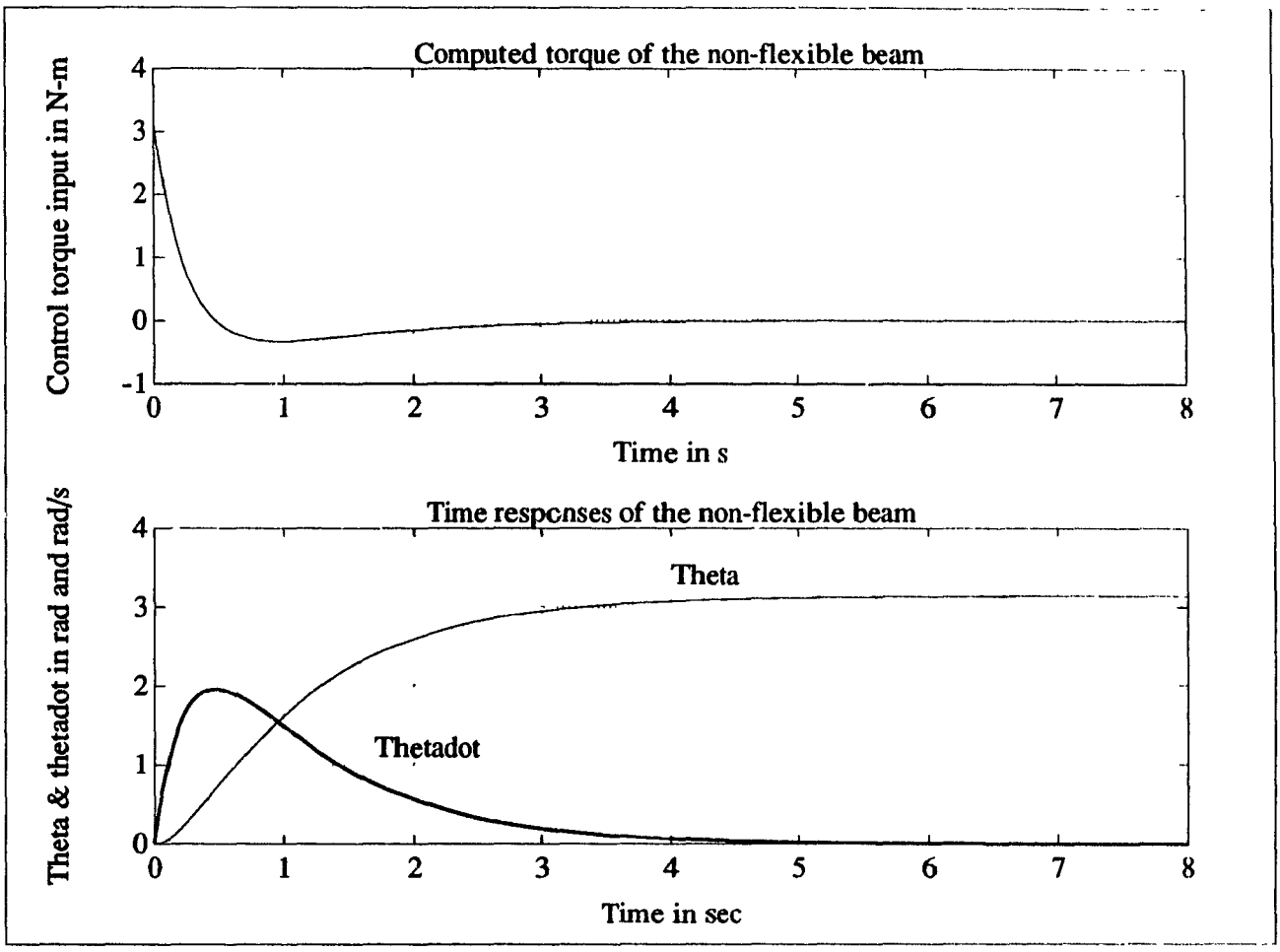

Figure 4.3: Optimal torque input and time responses of the non-flexible beam without tip mass

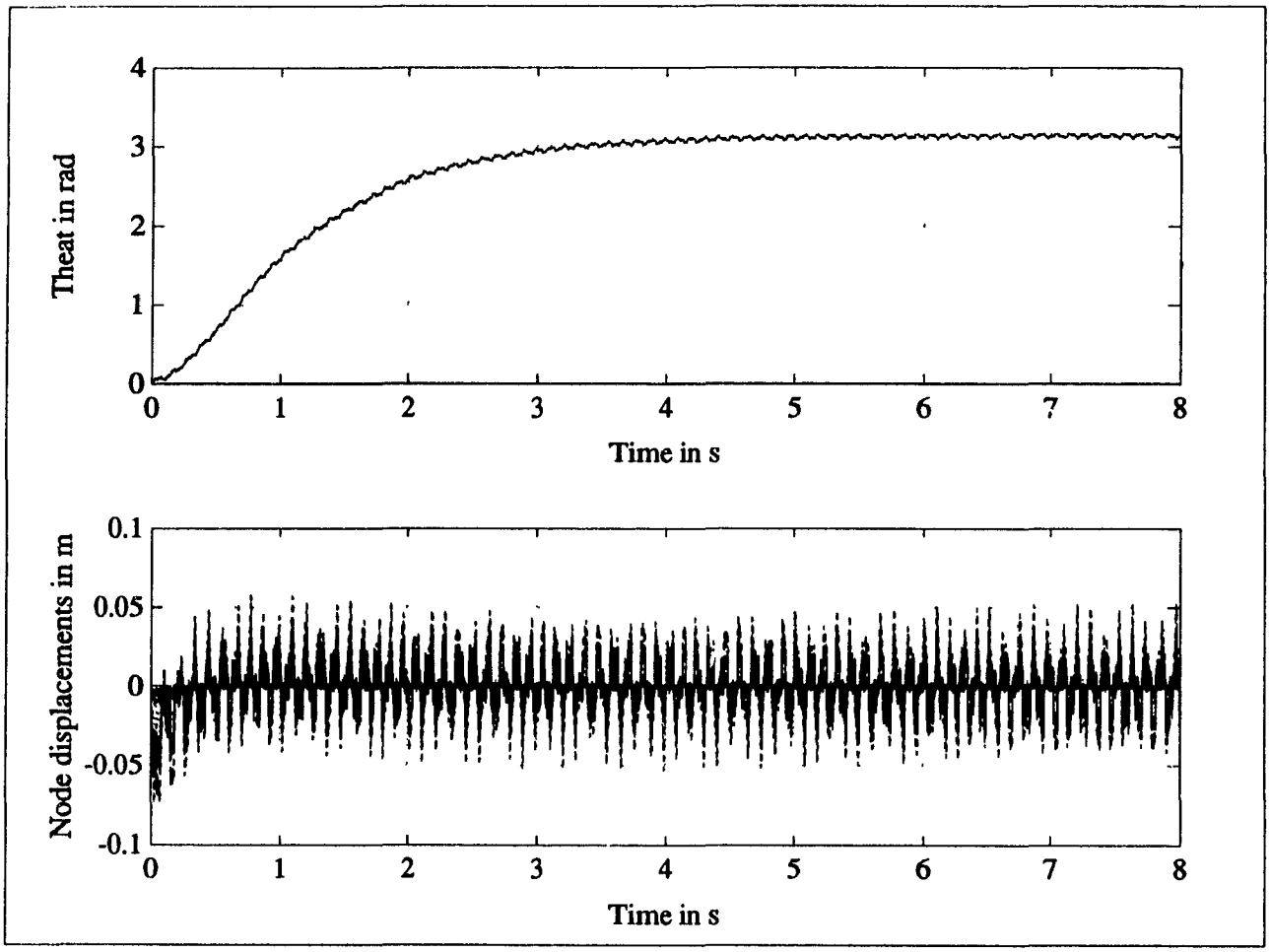

Figure 1.1: Time responses of the flexible beam for an optimal torque input of the rigid beam without tip mass

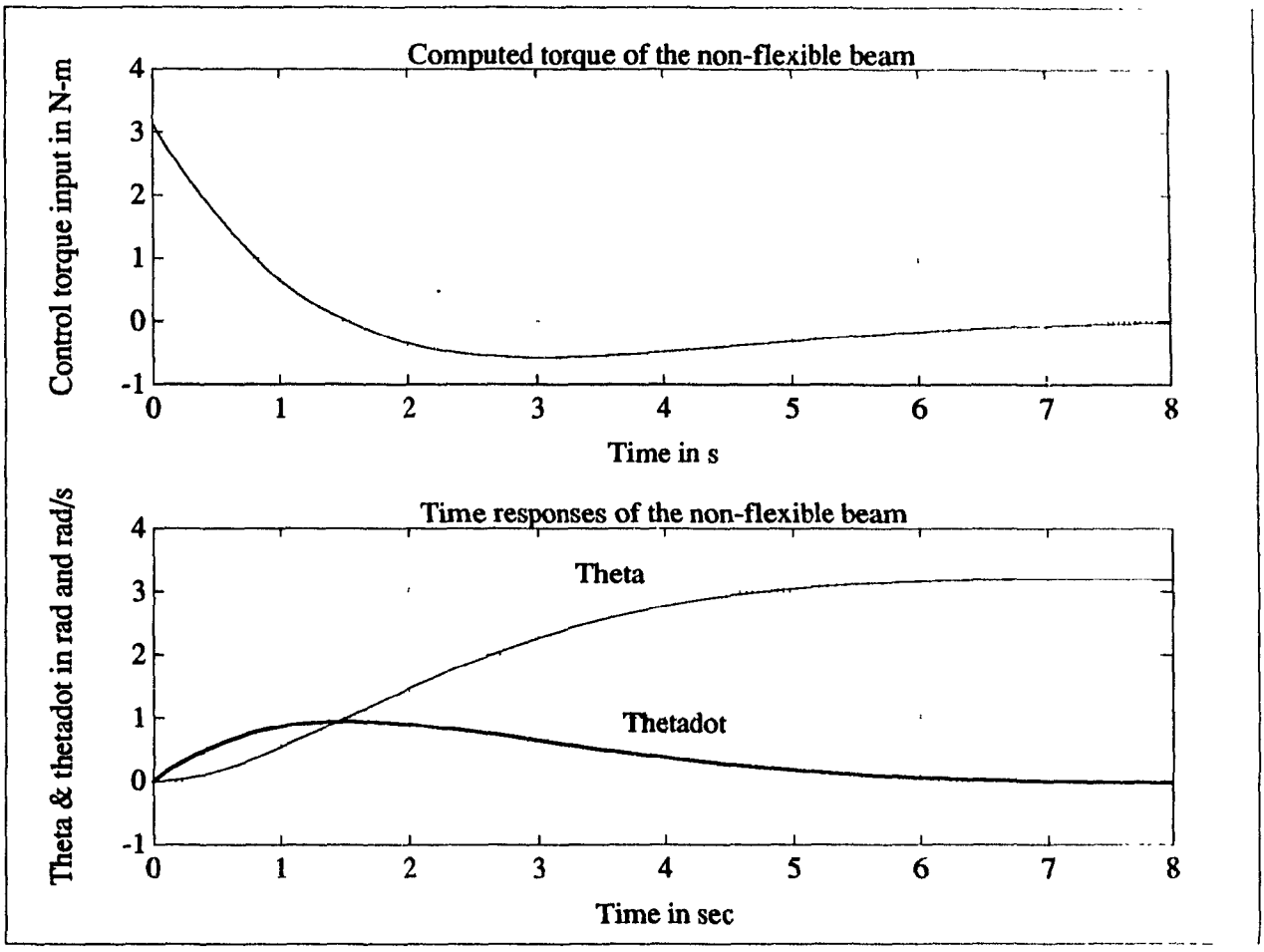

Figure 4.5: Optimal torque input and time responses of the non-flexible beam with tip mass

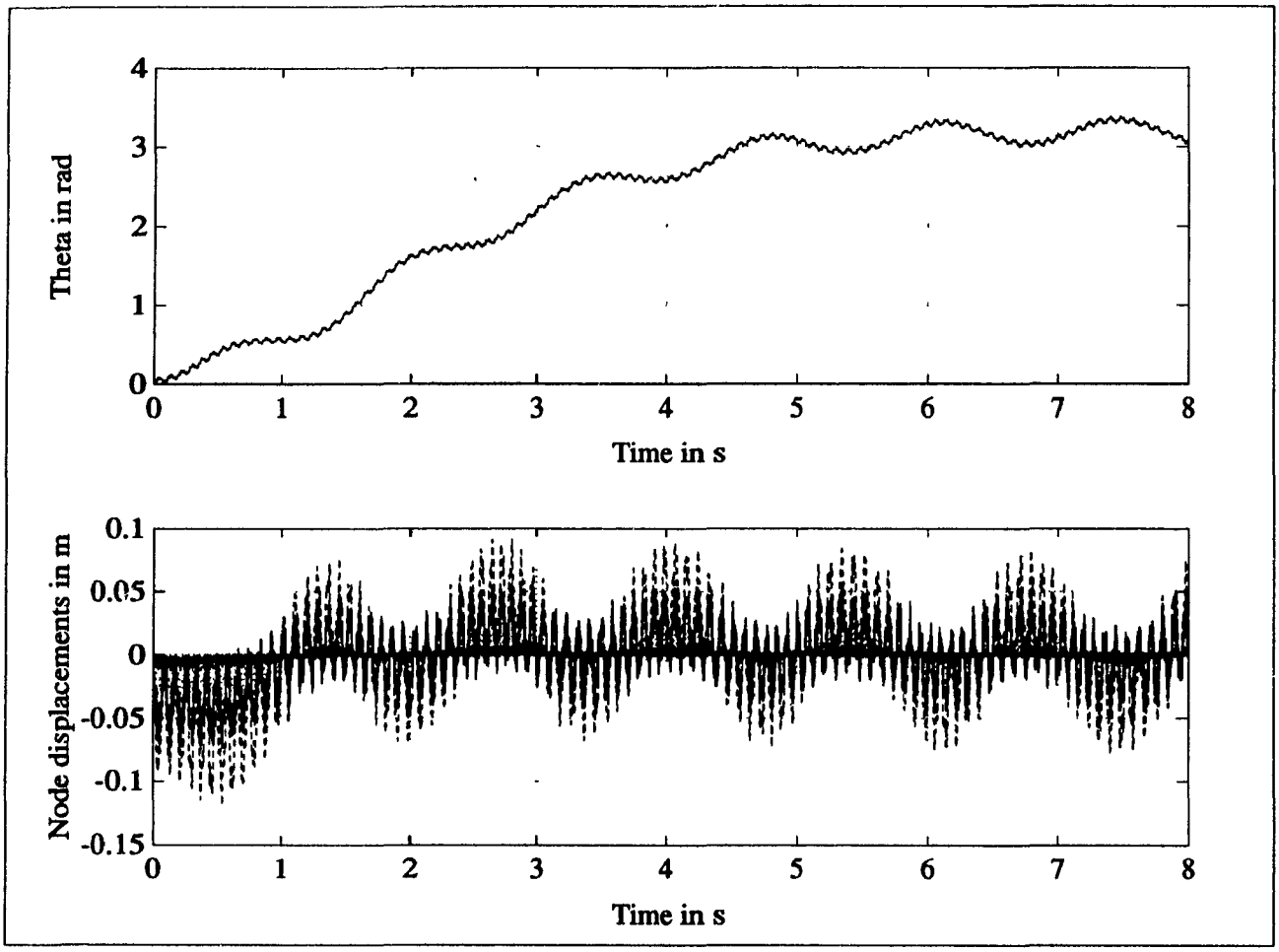

Figure 4.6: Time responses of the flexible beam for an optimal torque input of the rigid beam with tip mass

Table 4.5: The material specification of the beam

Number of nodal points (n)	7
Material	Aluminum
Mass density [kg/m^3]	2712
Young's modulus [GPa]	71.0
Moment of inertia of the hub [kg-m^2]	0.000831
Moment of inertia of the tip mass [kg-m^2]	0.90571986
Section moment of inertia of the beam [m^4]	2.25×10^{-10}
Moment of inertia of unflexed rigid beam [kg-m^2]	0.2712

4.5 Compensator Simulation

A simulation study was performed for the rotating flexible beam shown in Fig. 4.7 and described in Table 4.5, which exhibits high-frequency vibrations. A relatively high sampling rate of 500 Hz was chosen, based on the highest natural frequency of the beam to be controlled, for both control and measurement loops.

The initial conditions used were

$$\mathbf{q}(0) = \mathbf{0} \tag{4.10}$$

$$\dot{\mathbf{q}}(0) = \mathbf{0} \tag{4.11}$$

where $\mathbf{0}$ is the n-dimensional vector. Moreover, performing the calculations results in the

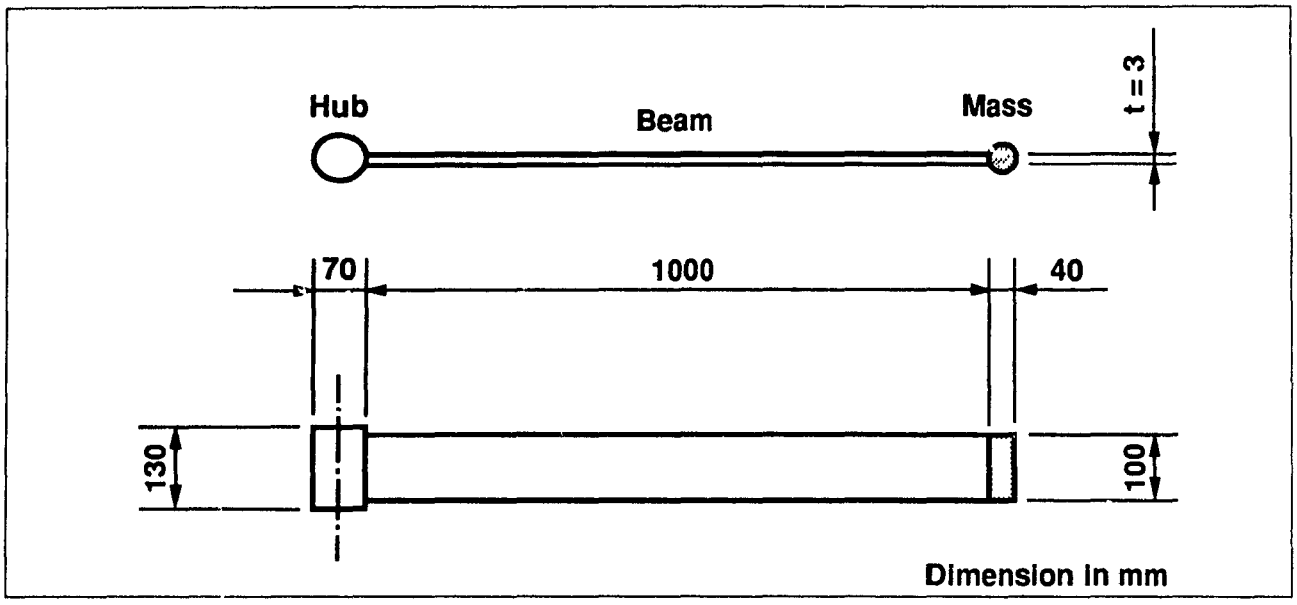

Figure 4.7: Beam used in simulation

steady-state, discrete-time, Kalman filter gain matrix $\mathbf{L}_\infty$ and controller gain vector $\mathbf{k}_\infty$

$$\mathbf{L}_\infty = \begin{bmatrix} 0.0095 & 0.0006 & -0.0037 \\ 0.0338 & 0.0010 & -0.0135 \\ -0.0069 & 0.0015 & -0.0137 \\ 0.0033 & 0.0007 & -0.0087 \\ -0.0084 & 0.0003 & -0.0022 \\ -0.0017 & 0.0009 & 0.0045 \\ -0.0037 & -0.0002 & 0.0716 \\ -35.6900 & 0.3392 & 1.0485 \\ 21.3990 & -0.4260 & -0.4360 \\ -7.7234 & 0.2005 & -0.3134 \\ 0.4238 & -0.0199 & -0.4091 \\ 3.6538 & -0.0043 & -0.2632 \\ -0.3160 & -0.0000 & -0.0083 \\ 1.6028 & 0.0011 & 0.0800 \end{bmatrix} \tag{4.12}$$

$$\mathbf{k}_{\infty}^{T} = \begin{bmatrix} 17.1077 \\ -12.0788 \\ 13.5363 \\ -1.9689 \\ 1.5337 \\ 0.8847 \\ 0.0176 \\ -0.0063 \\ 0.0028 \\ 0.0017 \\ -0.0053 \\ -0.0001 \\ -0.0018 \\ 0.0306 \end{bmatrix} \tag{4.13}$$

In order to avoid rapidly fluctuating system responses and, thus, to prevent the control signal from exceeding its physical limits, a smoothed step input using a cycloidal motion (Fig. 4.8) was employed to generate reference inputs for the hub rotational angle, θ_r, and its angular velocity, $\dot{\theta}_r$, namely,

$$\theta_r = \theta_0(\tau - \frac{1}{2\pi}\sin(2\pi\tau)), \tag{4.14}$$

$$\dot{\theta}_r = \theta_0(1 - \cos(2\pi\tau)),\ 0 \leq \tau \leq 1 \tag{4.15}$$

where θ_0 is the amplitude of the hub rotational angle. Consideration of the time rate of change for the given input offered the advantage of eliminating the small steady-state fluctuations of the response, at the expense of a slightly longer settling time.

The simulation of the flexible beam without tip mass was also performed to compare the results with those of the beam with tip mass (Fig. 4.9) and (Fig. 4.10) both with the measurement noise (See Appendix A). The mass at the tip had a mass equal to that of the beam. Without the mass at the tip, the optimal compensator showed that the settling time was approximately 3 seconds and neither overshoot nor undershoot appeared in the

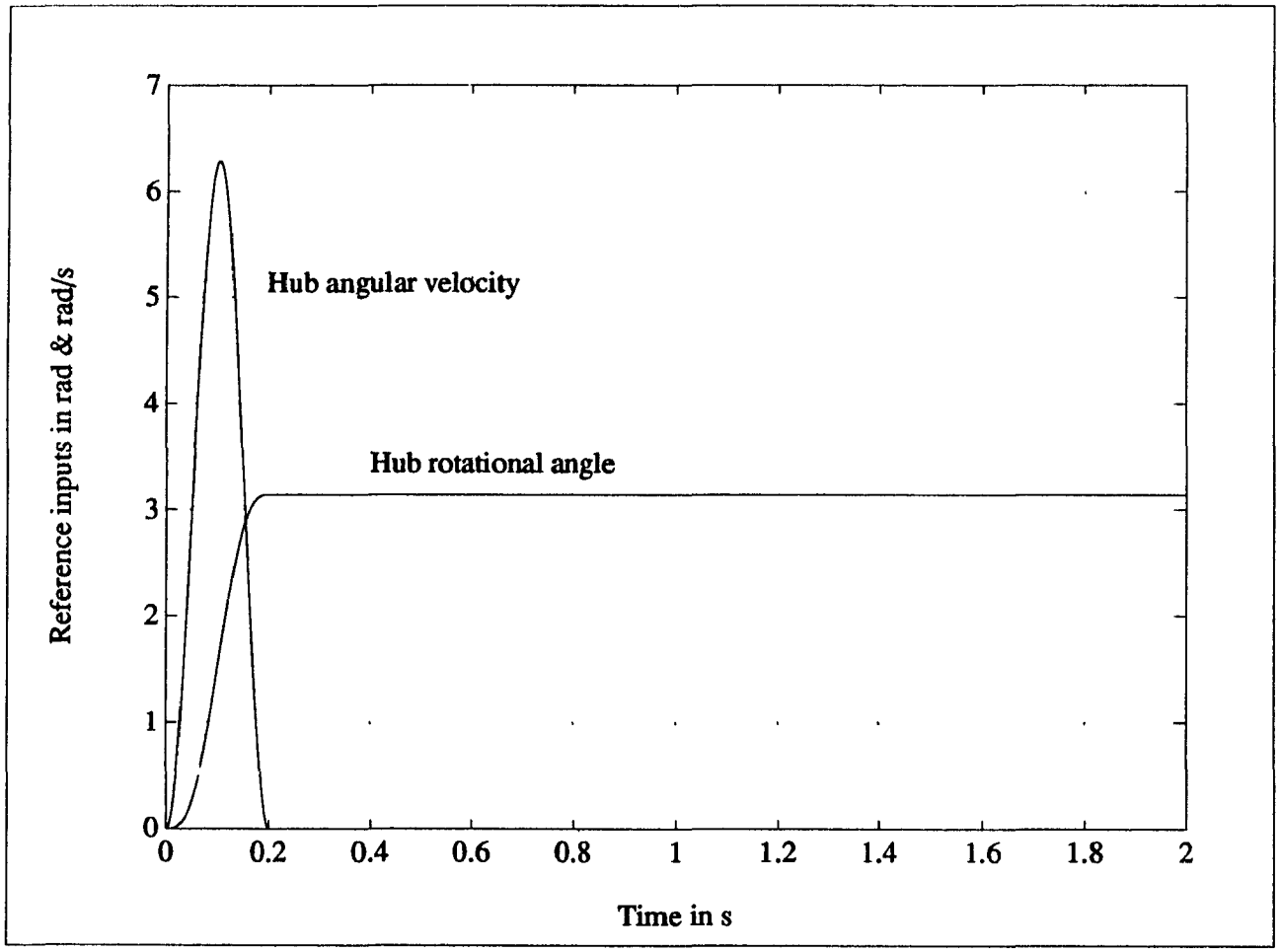

Figure 1.8: Smoothed step input using cycloidal motion

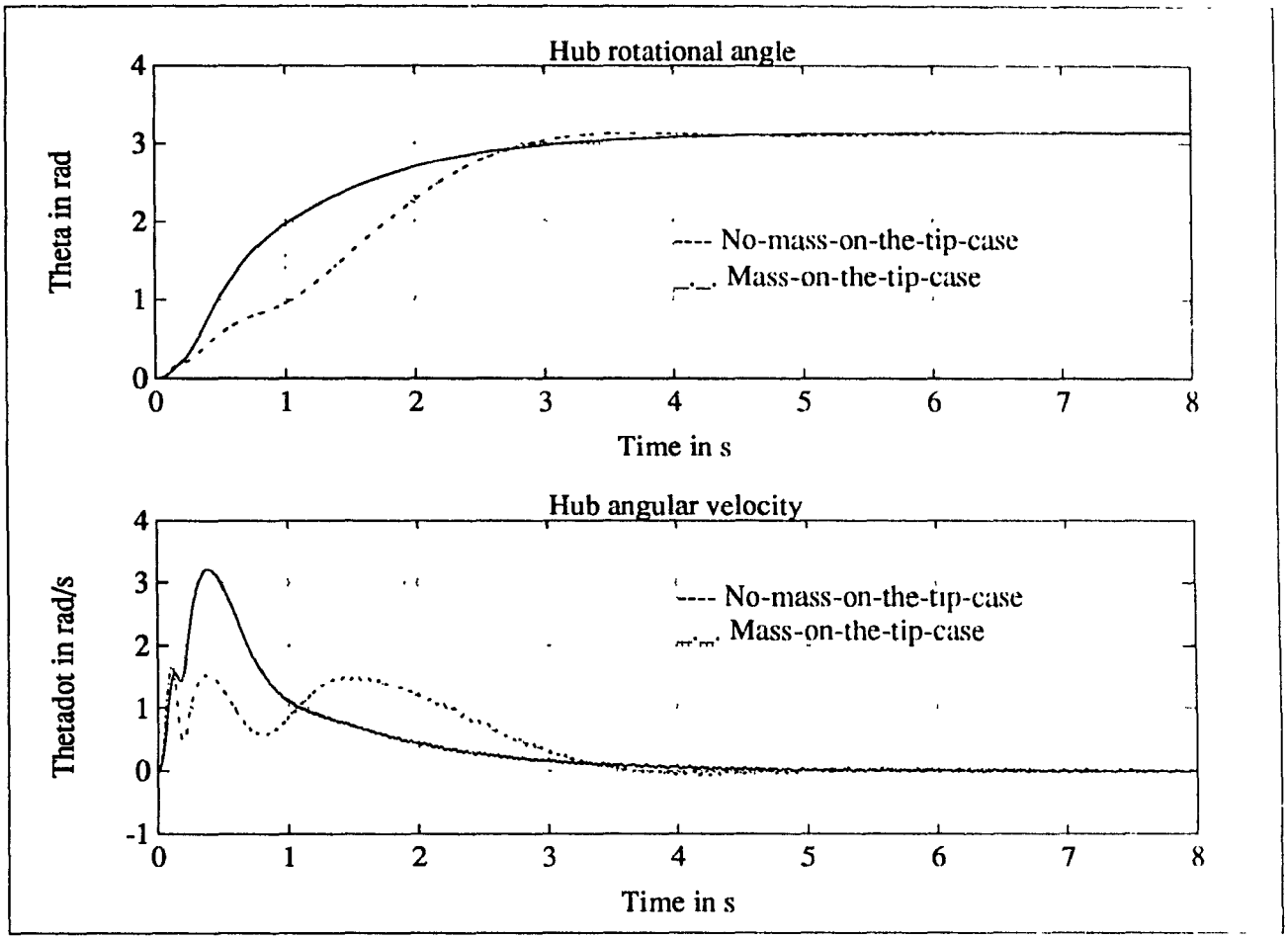

Figure 4.9: Hub rotational angle and its first time rate of optimally controlled rotating flexible beam

response of both the hub rotational angle and the hub angular velocity (Fig. 4.9). With the mass at the tip, comparatively small overshoot and undershoot with steady-state fluctuations occurred for the displacements at each nodal point (Figs. 4.9 and 4.10). However, it took longer for the response to settle due to the inertia of the tip mass, this being approximately 5 seconds. The comparison of control torque inputs for both cases is also shown in Fig. 4.11.

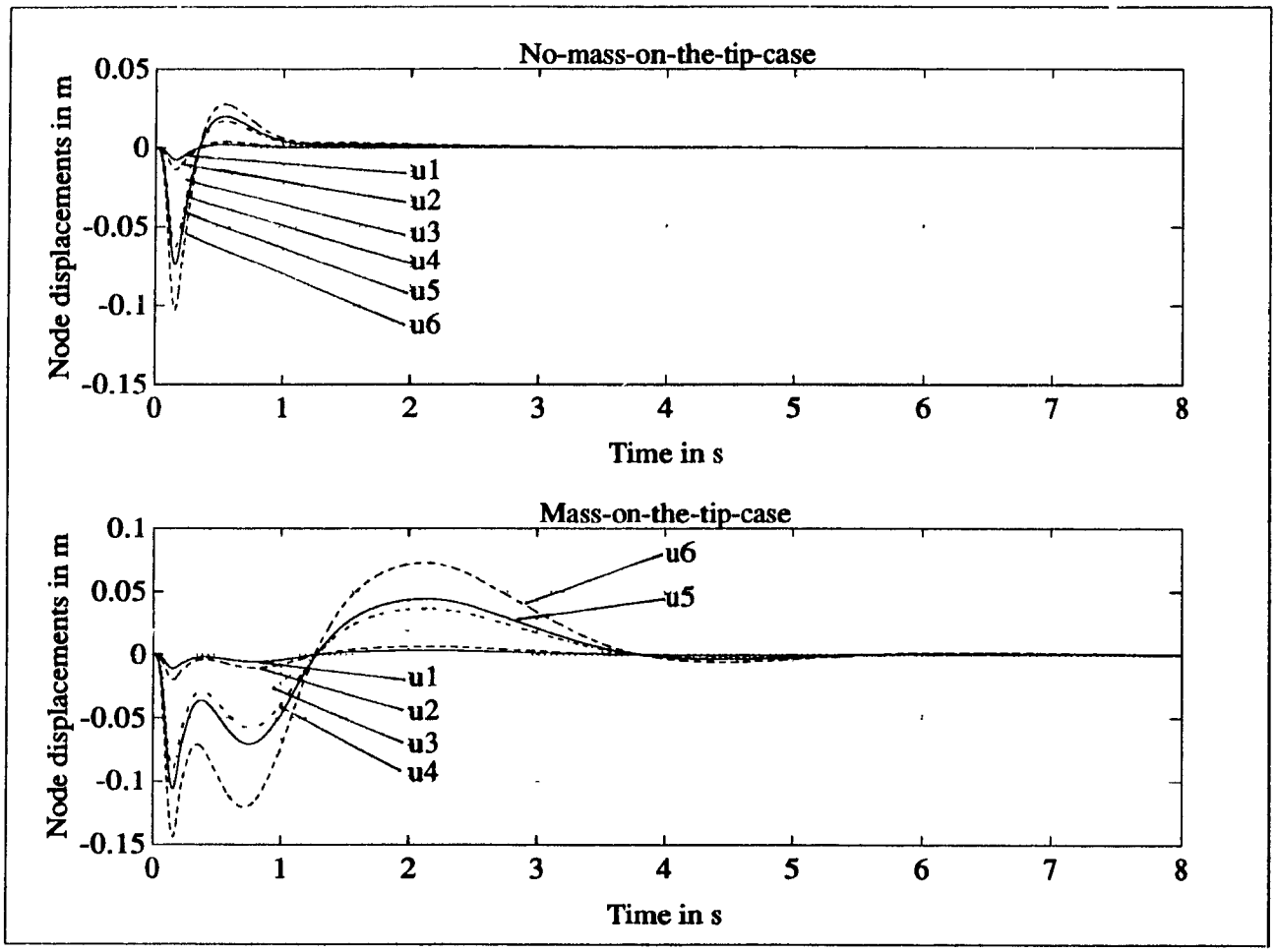

Figure 1.10: Node displacements of optimally controlled rotating flexible beam

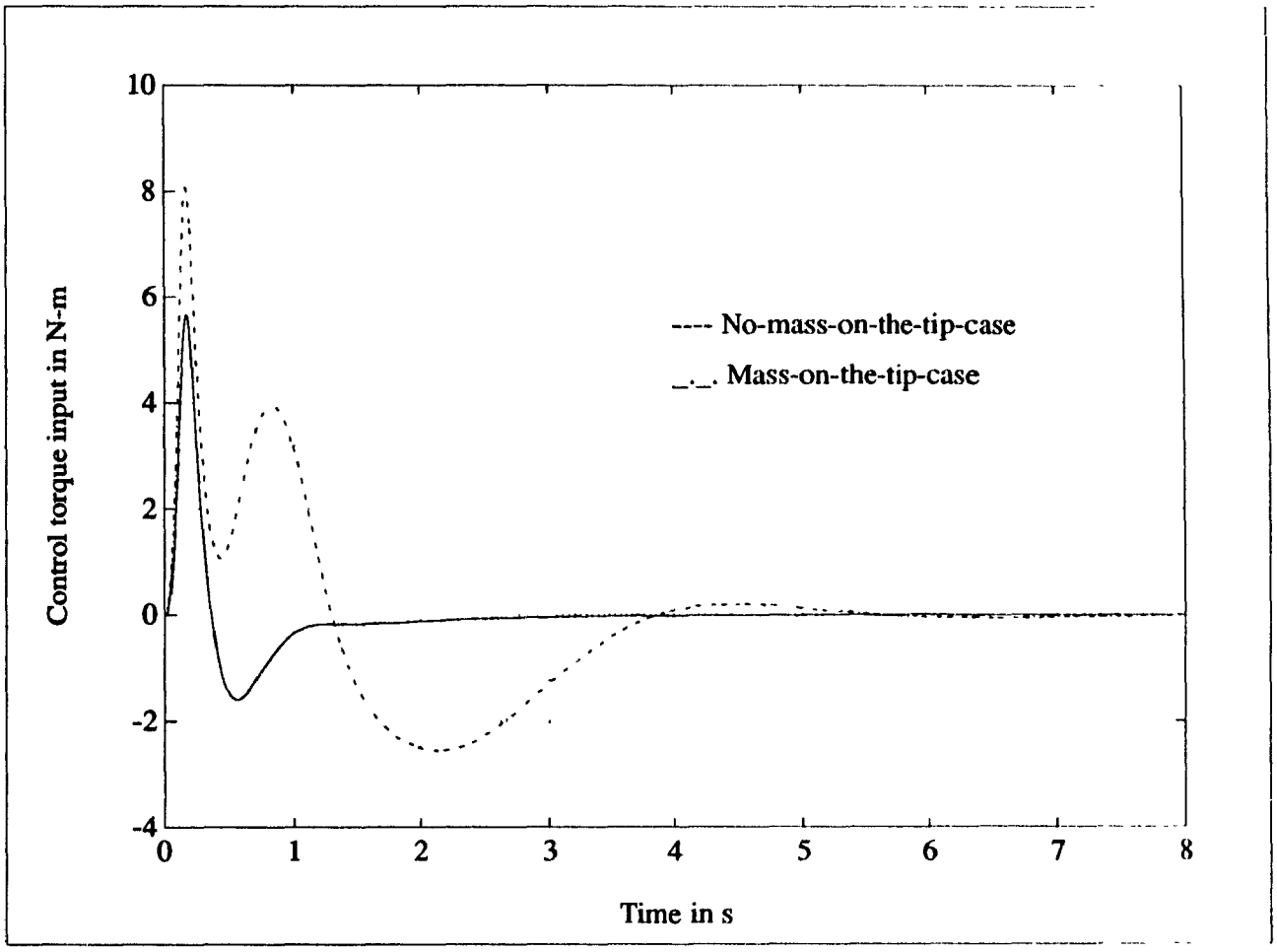

Figure 1.11: Comparison of optimal control inputs

Chapter 5

Conclusions and Suggestions for Further Work

A spatial discretization method using the cubic-spline technique has been proposed for the dynamic modelling of a continuous beam with a tip mass under large rigid-body motions. The major advantages of this approach lie in the capability of considering a variety of boundary conditions, as well as permitting the use of position sensors, rather than using vision systems. Moreover, this technique makes it possible to develop the dynamic modelling of nonuniform and nonsymmetric beams, which would be extremely difficult to model using an assumed-mode method.

Using the optimal controller with the Kalman filter, extensive simulations have been implemented to assess the feasibility of real-time control using the proposed modelling approach in the presence of measurement noise. Furthermore, the possibility of using a reduced number of curvature measurements is investigated. This includes the consideration of the state-observability and controllability of the sate-space system of the flexible beam associated with a smaller number of measurements. A practical and intuitive guideline for selecting the number and location of the sensors was given by finding maximum bending moment points for each of the modes up to the cutoff vibration mode, so that the system is state observable and gives the best estimations. It has been shown through extensive simulation studies that

measuring curvatures at the points which have maximum bending moment produces good estimations with a reasonable degree of accuracy. In addition, a high sampling rate is selected to avoid sensitive plant disturbances related to the high-frequency resonances. An optimal torque input of the closed loop system, assuming a rigid-body beam, was applied to the open-loop system of the flexible beam in order to examine the dynamic effects of link flexibility. The optimal control strategy scheme, using the Kalman filter and the cubic spline approximation technique is very suitable for on line control to suppress the transverse vibrations of a flexible beam undergoing large rigid body motions. An experimental setup is currently being built to test the theoretical work reported in this thesis.

A few extensions of this work to the following:

- Experimental verification of the proposed method.
- Use of the Euler operator (Hori, Nikiforuk and Kanai 1989; Middleton and Goodwin 1990).
- Extend the formulation to include two-dimensional bending effects and torsion effects accompanying multi-body motion.
- Develop an adaptive control algorithm to cope with changes of mass.

References

Astrom, K. J. and Wittenmark, B., 1984, *Computer-Controlled Systems. Theory and Design*, Prentice-Hall, Inc., New Jersey, Second edition.

Balas M., 1978, Feedback Control of Flexible Systems. *IEEE Transaction on Automatic Control*, Vol. AC-23, No. 1, pp. 673-679.

Balas M., 1982, Trends in Large Space Structure Control Theory: Fondest Hopes, Wildest Dreams. *IEEE Transaction on Automatic Control*, Vol. AC-27, No. 3, pp. 522-535.

Balas M., 1978, Modal Control of Certain Flexible Dynamic Systems. *SIAM Journal of Control and Optimization*, Vol. 16, No. 3, pp. 150-162.

Baruch H. and Choe K., 1990, Sensor Placement in Structural Control. *Journal of Guidance*, Vol. 13, No. 3, pp. 521-533.

Bayo, E., 1987, A Finite-Element Approach to Control the End-Point Motion of a Single-Link Flexible Robot. *Journal of Robotics System*, Vol. 4, No. 1, pp. 63-75.

Benati, M. and Morro, A., 1988, Dynamics of Chain of Flexible Links. *Journal of Dynamic System, Measurements, and Control*, Vol. 110, pp. 410-415.

Bishop R. E. D. and Johnson D. C., 1960, *The Mechanics of Vibration*, Cambridge University Press, New York.

Book W. J and Majette M., 1983 Controller Design for Flexible, Distributed Parameter Mechanical Arms Via Combined State Space and Frequency Domain Techniques. *Journal of Dynamic System, Measurements, and Control*, Vol. 105, pp. 245-251.

Cannon Jr., R. H. and Schmitz, E., 1984, Initial Experiments on the End-Point Control of a Flexible one-Link Robot. *The international journal of a Robotics Research*, Vol. 3, No. 3, pp. 62-75.

Dancose S., Angeles, J. and Hori, N., 1989, Optimal Vibration Control of a Rotating Flexible Beam. *ASME conference on Diagnostics, Vehicle Dynamics and Special Topics*, Montréal, pp. 259-261.

Dancose, S., 1987, Optimal Control and State Estimation of a Rotating Flexible Beam Master's Thesis, Department of Mechanical Engineering McGill University, Montréal, P.Q.

Dahlquist, J. and Björck, A., 1974, *Numerical Methods*, Prentice-Hall, Inc., New Jersey.

Davis, J. H. and Hirschorn, R. M., 1988, Tracking Control of a Flexible Robot Link *IEEE Transaction on Automatic Control*, Vol 33, No. 3, pp. 238-248

Giovagnoni M. and Rossi A., 1989, Transient Analysis of a Flexible Crank *Mechanism Machine Theory*, Vol. 24, No. 4, pp. 231-243.

Franklin, G., Powell, J. D. and Workman, M. L., 1990, *Digital Control of Dynamic Systems*, Addison-Wesley Publishing Company, Second edition.

Hori N, Nikiforuk P. N. and Kanni K.,1988, On a Discrete-Time System Expressed in the Euler Operator, *American Control Conference*, pp. 873-878, Pittsburgh, PA

Hughes P. C. and Skelton R. E., 1980, Controllability and Observability of Linear Matrix-Second-Order Systems, *Journal of Applied Mechanics*, Vol 47, pp. 415 420

Hughes P. C., 1987, Space Structure Vibration Modes: How Many Exist? Which Ones Are Important? *IEEE Control Systems Magazine*, Vol. 7, No 1, pp 22-28

Kailath T., 1980, *Linear Systems* Prentice-Hall, Inc., New Jersy.

Luenberger D. G., 1971, An Introduction to Observers, *IEEE Transaction on Automatic Control*, Vol. AC-16, No. 6, pp. 596-602.

Meirovitch, L., 1975, *Elements of Vibration Analysis* McGraw Hill, New York

Meng, C.-H. and Chen, J.-S., 1988, Dynamic Modeling and Payload Adaptive Control of a Flexible Manipulator, *IEEE Robotics and Automation*, pp 188 193

Middleton R. H. and Goodwin G. C., 1990. *Digital Control and Estimation*. Prentice-Hall, Inc., New Jersey.

Sakawa, Y., Matsuno, F. and Fukushima, S., 1985. Modeling and Feedback Control of Flexible Arm *Journal of Robotics System*, Vol. 2, No. 1, pp. 153-172.

Salgado, M., Middleton, R. and Goodwin, G. C., 1988, Connection between continuous and discrete Riccati equations with application to Kalman filtering. *IEE Proceedings*, Vol. 135, Pt. D, No. 1, pp.28-31.

Shchuka A. and Goldenberg A. A., 1989, Tip Control of a Single-Link Flexible Arm Using a Feedforward Technique. *Mechanism Machine Theory*, Vol. 21, No. 5, pp. 139-155.

Späth, H., 1978, *Splines Algorithmen zur Konstruktion glatter Kurven und Flachen*, R. Oldenbourg Verlag, Second edition.

Timoshenko, S., 1955, *Vibration Problems in Engineering*, Van Nostrand, Princeton, New Jersey.

Torfs D., Swevers J. and Schutter De J., 1991, Quasi-Perfect Tracking Control of Non-Minimal Phase Systems. Internal Report 91P55 of Katholieke Universiteit Leuven, Belgium.

Appendix A

Derivation of Noise Covariance Matrices

$\mathbf{R}_v$ and $\mathbf{R}_e$, the discrete-time measurement and process noise covariance matrices, respectively, are defined as

$$\mathbf{R}_v = E\{\mathbf{v}(k)\mathbf{v}(k)^T\} \tag{A.1}$$

$$\mathbf{R}_e = E\{\mathbf{e}(k)\mathbf{e}(k)^T\} \tag{A.2}$$

Moreover, they can be approximated by using the continuous-time covariance matrices as follows (Salgado, Middleton and Goodwin 1988):

$$\mathbf{R}_v \simeq \Delta E\{\mathbf{v}(t)\mathbf{v}(t)^T\} \equiv \Delta \mathbf{R}_{cv} \tag{A.3}$$

$$\mathbf{R}_e \simeq \frac{1}{\Delta} E\{\mathbf{e}(t)\mathbf{e}(t)^T\} \equiv \frac{1}{\Delta}\mathbf{R}_{ce} \tag{A.4}$$

where Δ is the sampling interval.

Let us choose n-dimensional noise vector $\mathbf{w}(t)$ to model the measurement and process noise as

$$\mathbf{w}(t) = \begin{bmatrix} k_1 x_1 \\ k_2 x_2 \\ \vdots \\ k_n x_n \end{bmatrix} \tag{A.5}$$

where x_i is a normally distributed random variable having zero mean and unit variance, and κ_i is a constant which is used to define the amplitude of the noise. The corresponding noise covariance matrix $E\{\mathbf{w}\mathbf{w}^T\}$ is clearly given as

$$E\{\mathbf{w}\mathbf{w}^T\} = \begin{bmatrix} \kappa_1^2 & 0 & \cdots & 0 \\ 0 & \kappa_2^2 & \cdots & 0 \\ \vdots & & \ddots & \vdots \\ 0 & 0 & \cdots & \kappa_n^2 \end{bmatrix} \tag{A.6}$$

Therefore, matrices $\mathbf{R}_{xy}$ and $\mathbf{R}_{xx}$ can be evaluated from the above covariance matrix.